Photopolymerization and 3D/4D applications using newly developed dyes: Search around the natural chalcone scaffold in photoinitiating systems

Hong Chen, Guillaume Noirbent, Yijun Zhang, Ke Sun, Shaohui Liu, Damien Brunel, Didier Gigmes, Bernadette Graff, Fabrice Morlet-Savary, Pu Xiao, et al.

Photopolymerization and 3D/4D applications using newly developed dyes: Search around the natural chalcone scaffold in photoinitiating systems

Hong Chen [a,b], Guillaume Noirbent [c], Yijun Zhang [a,b], Ke Sun [a,b], Shaohui Liu [a,b], Damien Brunel [c], Didier Gigmes [c], Bernadette Graff [a,b], Fabrice Morlet-Savary [a,b], Pu Xiao *[d], Frédéric Dumur * [c], Jacques Lalevée * [a,b]

[a] Université de Haute-Alsace, CNRS, IS2M UMR 7361, F-68100 Mulhouse, France

[b] Université de Strasbourg, France

[c] Aix Marseille Univ, CNRS, ICR UMR 7273, F-13397 Marseille, France; frederic.dumur@univ-amu.fr

[d] Research School of Chemistry, Australian National University, Canberra, ACT 2601, Australia; pu.xiao@anu.edu.au

* Corresponding author: jacques.lalevee@uha.fr (J. L.), frederic.dumur@univ-amu.fr (F. D.); pu.xiao@anu.edu.au (P. X.).

Abstract: Two series of 18 new dyes selected from in silico molecular design (i.e. through molecular orbital calculations) were synthesized and used in conjunction with an amine (i.e. ethyl l,4-(dimethylamino)benzoate, EDB) and an iodonium salt (*bis*(4-*tert*-butylphenyl)iodonium hexafluorophosphate, Iod) as photoinitiating systems (PISs) capable of initiating the free radical polymerization of polyethylene glycol (600) diacrylate (PEG-diacrylate) and the cationic polymerization of 3,4-epoxycyclohexylmethyl-3,4-epoxycyclohexanecarboxylate (EPOX) via an oxidation–reduction reaction mechanism. Even though most of these dyes exhibit excellent light absorption properties below 380 nm, the photopolymerization efficiency of acrylates carried out under LED@405 nm are much better than that reached with a LED@375 nm both in thin films and thick films. Furthermore, all of them can also boost the cationic polymerization of EPOX upon LED irradiation at 405 nm, in the presence of

an iodonium salt and an amine. More interestingly, stereoscopic 3D patterns were successfully fabricated by the laser writing technique which demonstrated reversible swelling properties and reversible shape-memory effects induced via swelling and dehydration for the access to 4D printing.

Keywords: Natural dyes; photopolymerization; 3D/4D printing; thermoresponsive and water-responsive reversible shape-memory

1. Introduction

Photopolymerization under mild light conditions such as visible light is still an active research area which requires the development of new high-performance photoinitiators [1-6]. With aim at optimizing the polymerization ability of the photoinitiator, not only the light absorption properties of the chromophore need to be considered, the other parameters such as the rate constant of interaction of photoinitiators with the different additives introduced into the photocurable resins, the excited state lifetimes and energies, the redox potentials etc. are also important and undoubtedly govern the polymerization efficiency [7-11].

Even if a number of studies have shown that some natural dyes can be used as non-toxic photoinitiators to induce a photopolymerization due to the highly conjugated nature of their skeletons, their good biocompatibilities and stabilities made them ideal candidates for the elaboration of biomaterials and other materials of related applications. In this context, these natural dyes have attracted a great deal of interest in various research fields [12-14]. The natural dyes can easily initiate an electron transition from the ground state to the excited state after absorbing the appropriate light and thus generate the active species (e.g. cations or free radicals) that can initiate some polymerization reactions through electron (or energy) transfer between themselves or with other additives. Their reactivities are closely related to their photochemical properties that depend of their chemical structures [15-17].

Parallel to the photoinitiating ability, another active research field concerns the shape-memory effect of the polymers which has drawn considerable research interest

in the last few years because of their widely applications [18-20]. Benefiting from their flexibility, biocompatibility and unlimited possibility of chemical modifications, the shape memory polymers (SMP) materials clearly prove to be suitable substitutes to metallic materials [21-23]. SMP materials are stimuli-responsive materials, which have the capability of changing their shapes upon application of an external stimulus such as heat [24,25], light [26], electric field [27], magnetic field [28] or water [29,30]. The shape-memory effect is not dependent of a specific material property of the single polymers; It results from a subtle interplay between the polymer structure and the polymer morphology together with the applied processing and programming technology. The process of programming and recovery of a shape is shown in the following steps: first, the polymer is conventionally processed to receive its permanent shape; afterwards, the polymer is deformed and fixed the intended temporary shape under external stimuli (the process is called programming); finally, withdrawing the stimulus used before or applying another stimulus will induce the shape-memory effect so that the recovery of the stored temporary shape can be observed. By further programming, including mechanical deformation, the work piece can be brought into a temporary shape again that is called the reversible shape memory effect, while it's named as a one-way shape-memory effect if no recovery of the temporary shape can be observed [31-33].

Concerning the abovementioned requirements, two series of 18 new dyes with excellent light absorption properties were selected from in silico molecular design (i.e. through molecular orbital calculations) and firstly studied as photoinitiators for FRP and CP in this work. More specifically, their photopolymerization abilities were investigated in conjunction with an amine (EDB) and an iodonium salt (Iod) as photoinitiating systems (PISs) activable with LEDs emitting at 405 nm and 375 nm which allowed an efficient comparison of their performances. Parallel to monitoring the polymerization kinetics, steady state photolysis experiments were performed to characterize the excited state reactivity of the dyes. The photochemical mechanism involved in the polymerization process was also studied in detail through steady-state fluorescence quenching and electron spin resonance (ESR) experiments as well as the

calculation of free energy changes. Finally, to evidence the interest in these new structures, 3D printing experiments were carried out using the newly proposed photoinitiation systems, and stereoscopic 3D patterns were successfully fabricated. These patterns demonstrated reversible swelling properties and reversible shape-memory induced via swelling and dehydration for the access to 4D printing.

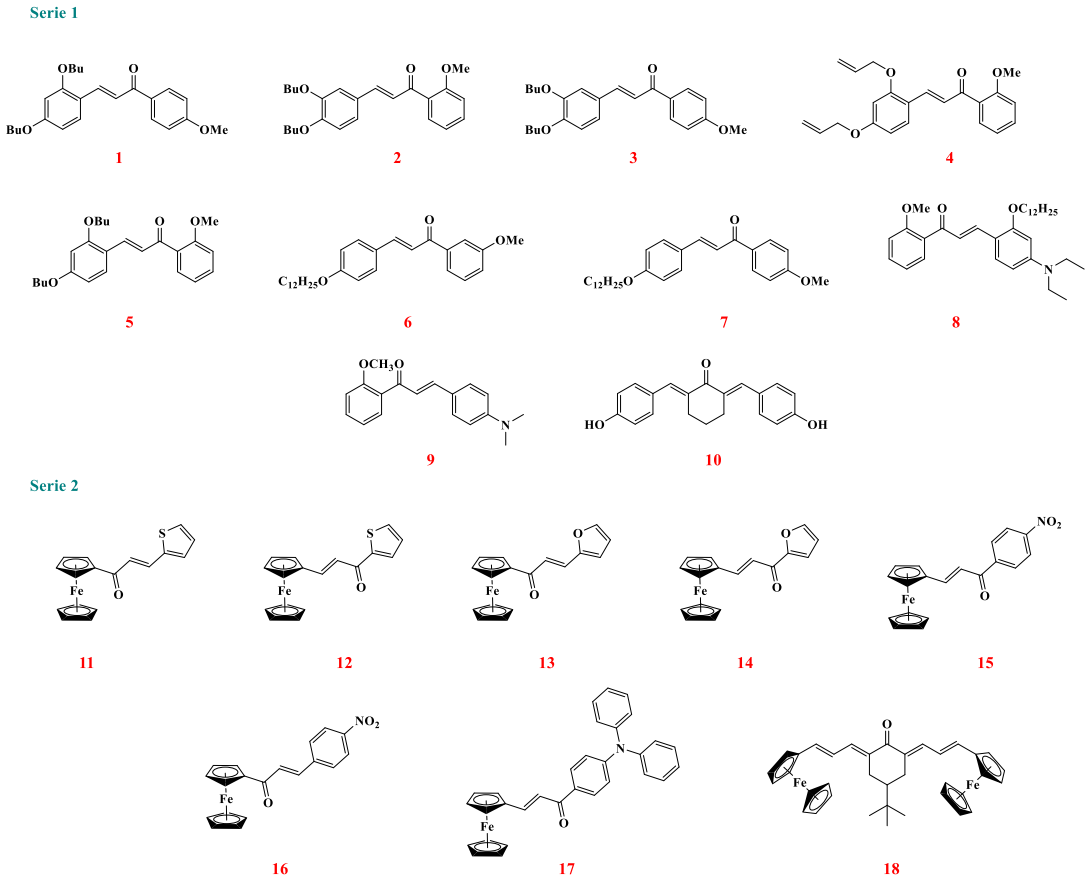

Scheme 1. Chemical structures of dyes 1-18 studied in this work: (Series 1, dyes 1-10) alkoxy-based chalcones and (Series 2, dyes 11-18) ferrocene-based chalcones.

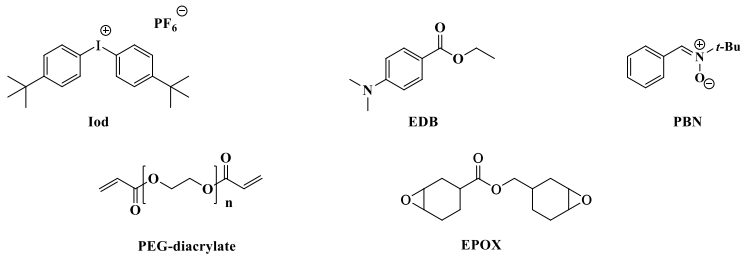

Scheme 2. Chemical structures of the iodonium salt (Iod; Speedcure 938), the amine (EDB; Speedcure EDB), Phenyl-*N*-*tert*-butylnitrone (PBN) and the functional benchmark monomer (PEG-diacrylate and EPOX).

2. Materials and Methods

2.1 Materials

The 18 chalcone-based photoinitiators were prepared as described in the SI† and their chemical structures are shown in Scheme 1. The free radical photopolymerization monomers used in this work, namely, polyethylene glycol (600) diacrylate (PEG-diacrylate: SR 610) and polyethylene glycol (400) diacrylate (PEG-diacrylate: SR 415) were purchased from Sartomer-Europe. The cationic photopolymerization monomer, 3,4-epoxycyclohexylmethyl-3,4-epoxycyclohexanecarboxylate (commercially known as EPOX or Uvacure 1500) was purchased from Allnex. The spin trap agent phenyl-*N*-*tert*-butylnitrone (PBN), the supporting electrolyte tetrabutylammonium hexafluorophosphate, the co-initiator (*bis*-(4-*tert*-butylphenyl)iodonium hexafluorophosphate, Iod; Speedcure 938) and the electron donor (ethyl 4-(dimethyl-amino)benzoate, EDB; Speedcure EDB) were all purchased from Sigma-Aldrich, and their corresponding molecular structures are shown in Scheme 2. The solvent (i.e. acetonitrile and *tert*-butylbenzene) were also purchased from Sigma-Aldrich and were all of analytical grade.

2.2. Molecular Modeling

The Gaussian 03 suite of programs was used for the molecular orbital calculations. Furthermore, the time-dependent density functional theory at the MPW1PW91/6-31G* level and the theory on the relaxed geometries at the UB3LYP/6-31G* level was used to simulate the UV-visible absorption spectra and calculate the triplet state energy levels of the two series of dyes [34-35].

2.3. Photochemical Properties of the Dyes

2.3.1. UV-Visible Absorption Spectroscopy

In this work, the UV-visible absorption properties and the photolysis experiments of the proposed dyes were investigated through a JASCO V730 UV–visible spectrometer. The dyes were dissolved in acetonitrile and the solutions were prepared with the concentration about 5×10^{-5} M. In addition, a LED@405 nm was used as the light source for the photolysis experiments, and the concentration of Iod and EDB are

all kept at 0.1 M.

2.3.2. The Electron Transfer Reaction for Dyes Characterized by Fluorescence Experiments

For the fluorescence properties, the dyes were analyzed in acetonitrile with a concentration of 5 $\times 10^{-5}$ M by a JASCO FP-6200 spectrofluorimeter.

2.3.3. Electron Spin Resonance Spin Trapping (ESR-ST) Experiment of the Dyes

An X-band spectrometer (Bruker EMXplus) was used for the electron spin resonance (ESR) spin trapping experiments. The generated free radicals of different samples were trapped in nitrogen-saturated *tert*-butylbenzene solution at room temperature. A LED @ 405 nm was used as the light radiation source and *N*-*tert*-butyl-α-phenylnitro (PBN) was used as the spin trapping agent. ESR spectra simulations were carried out using the WINSIM software [36].

2.3.4. Cyclic Voltammetry of the Dyes.

The redox potentials (oxidation potential E_{ox} vs. SCE and reduction potential E_{red} vs. SCE) for the selected dyes were measured in acetonitrile by cyclic voltammetry. For this experiment, tetrabutylammonium hexafluorophosphate (Aldrich) was used as the supporting electrolyte; a platinum electrode was used as a working electrode and a saturated calomel electrode (SCE) was used as the reference electrode [37,38]. Furthermore, the free energy change of the singlet state for the electron transfer reaction was calculated from Equation (1) or Equation (2); similarly, for the triplet state, the free energy change was calculated from Equation (3) or Equation (4) , which determined by E_{ox} , E_{red} , E_{S1} and E_{T1}. Here, E_{ox} is the oxidation potential of the electron donor (EDB), E_{red} is the reduction potential of the electron donor (EDB), E_{red} is the reduction potential of the electron acceptor (Iod), E_{S1} is the excited state energy level (calculated from the crossing point of UV-visible and fluorescence spectra) and E_{T1} is extracted from molecular energy level calculations (Gaussian 03 suite of programs). In addition, the reduction potential of iodonium was − 0.7eV and the oxidation potential of EDB was

1.0eV according to the literature data [39].

$$\Delta G^{S1}_{Iod} = E_{ox} - (-0.7) - E^{*}_{S1} \quad (1)$$

$$\Delta G^{S1}_{EDB} = 1.0 - E_{red} - E^{*}_{S1} \quad (2)$$

$$\Delta G^{T1}_{Iod} = E_{ox} - (-0.7) - E^{*}_{T1} \quad (3)$$

$$\Delta G^{T1}_{EDB} = 1.0 - E_{red} - E^{*}_{T1} \quad (4)$$

2.4. Photopolymerization Experiments

2.4.1. Photopolymerization Kinetics Monitored by Real-Time Fourier Transform Infrared Spectroscopy (RT-FTIR) using LEDs at 375nm or 405nm

In order to examine the influence of the three-component photoinitiating systems on both the free radical photopolymerization (FRP) and the cationic photopolymerization, both photoinitiators (chalcones) and additives, namely the iodonium salt (Speedcure 938) and the electron donor (Speedcure EDB), were prepared separately in order to fulfill the following conditions (chalcones/Iod/EDB: 0.5%/1.5%/1.5% w/w/w). The weight contents of each component were calculated from the monomers (PEG-diacrylate or EPOX) content. Moreover, the photosensitive formulations of all samples were dropped between two polypropylene films (thickness ~20 μm) with one drop of resin in laminate for the FRP, sandwiching the formulation in the middle to reduce the O_2 inhibition. For the CP of EPOX films (thickness ~20 μm) the experiments were carried out under air using a polished polypropylene film as substrate with one drops of resin. As a blank control, the monomer (1 g, PEG-diacrylate or EPOX) and only the additives, i.e. the iodonium salt (Speedcure 938, 1.5%, w/w) and the electron donor (Speedcure EDB, 1.5%, w/w), were tested under the same conditions as those used for the three-component systems. Evolution of the epoxy or the acrylate functions content was continuously monitored by real time Fourier transform infrared spectroscopy (RT-FTIR, JASCO FTIR 4100) at the characteristic peaks around 790 cm^{-1} and 1630 cm^{-1}, respectively, under LED 375nm or 405nm [40].

2.4.2. Laster writing Experiment

A computer-programmed laser diode (Thorlabs) with a spot size of about 50 μm, and LED @ 405 nm as a light radiation source was used to produce the specific three-dimensional patterns while using the newly developed three-component photoinitiating systems with PEG-diacrylate. The compound was deposited into a homemade model (2 mm thickness) and different laser writing speeds were studied. Finally, the printed 3D patterns were analyzed by a numerical optical microscope (DSX-HRSU, Olympus).

2.5. 4D Printing Applications

2.5.1. Swelling Kinetics of 3D Patterns Produced by Proposed Three-Compound Photoinitiating Systems based on dyes/Iod/amine with PEG-diacrylate

The swelling kinetics of the "**T**" 3D printed patterns prepared from the three-component PISs based on dyes/Iod/amine (0.5%/1.5%/1.5%, w/w/w) of PEG-diacrylate monomers were tested in quintuplicate (n = 3) were weighed and placed in glass bottles filled with residual water for 24h to reach the swelling equilibrium. The samples were then removed and the residual water at the surface of them was blotted with filter paper. Thereafter, the wet weight of each polymerization product was measured (Wt) and compared to the initial wet weight (Wo), the swelling ratio (*Sr*) was defined by eq (5). Furthermore, the volume of each samples was measured (Vt) and compared to the initial volume (Vo), the increase ratio of volume after swelling (*Vr*) was defined by eq (6). After that, the swelled patterns were placed into an oven at 50°C for 0.5h to remove the absorbed water [41,42].

$$\textbf{Swelling Ratio (\%)} = (W_t - W_o) / W_o \times 100 \quad (5)$$

$$\textbf{Volume Changed Ratio (\%)} = (V_t - V_o) / V_o \times 100 \quad (6)$$

2.5.2. Shape-Memory of Polymers through Thermo-Responsive and Water-Responsive.

The shape-memory and reversible deformation effect of the PEG-polymer prepared with the proposed three-component PISs based on dye 6/Iod/amine (0.5%/1.5%/1.5%, w/w/w) upon irradiation with a LED@395 nm were induced by swelling and dehydration sequences following this procedure: firstly immersing the

polymerization products in water at room temperature for 2 min to swell; secondly, moving them into a 80°C incubator and heating for 10 min to remove the soaked water; finally, keeping the products at room temperature to restore the corresponding initial shape.

3. Results

3.1. Free radical polymerization (FRP) kinetics of PEG-diacrylate.

For the polymerization of the acrylate monomer PEG-diacrylate, the photoinitiation abilities of the two series of dye-based three-component PISs (from dye 1 to 18) were investigated using real-time Fourier transform infrared spectroscopy (RT-FTIR) within the same LED irradiation time (200 s) at room temperature, as shown in Figure 1. First, all the dye (1-18)-based three-component PISs dye/Iod/amine (0.5%/1.5%/1.5%) were tested in thin films under irradiation with a LED@405nm in laminate (the thickness is about 0.1mm, see in Figure 1 a and b), most of the resulting photoinitiating systems could lead to final double bond conversions of monomer exceeding 80%, which are higher than the blank control that only contains Iod and EDB (1.5%/1.5%, w/w, 76%). Under the same conditions, we also examined the photopolymerization efficiencies of all dyes (1-18) based three-component PISs dye/Iod/amine (0.5%/1.5%/1.5%) for the polymerization of thick films (the thickness is about 2 mm, see in Figure S1 a and b), but only dyes 3, 6 and 7 (98%, 93%, and 96%, respectively) based systems showed better efficiencies than that of the blank control (93%). As depicted in the Figure 1, typical double bond conversions vs irradiation time profiles indicate that the presence of the dyes is essential to promote the free radical photopolymerization process, based on the comparison established with the Iod/amine two-component systems.

Due to their strong absorptions in the ultraviolet region i.e. below 380 nm except for dyes 8 and 9 whose maximum wavelength are around 400-410 nm, photoinitiating ability of the same photoinitiating systems were tested at shorter wavelength and a LED@375nm was used as the irradiation light source for these new experiments. As shown in Figures 1 c and d, even though the polymerization rate of most of the

photoinitiating systems are faster than the blank control for thin films, the final conversions for all of them remained below 80%, which is extremely low in comparison of the final monomer conversion obtained with the blank control (94%) and that obtained upon irradiation with a LED@405nm (⩾80%). In addition, for the thick films (the thickness was about 2 mm, see in Figures S1 c and d), no curing in depth was observed for most of the dyes-based systems. Additionally, the polymerization efficiency of these deep-cured systems was much lower than that of the blank control. The above results indicate that the irradiation condition has a huge effect on the polymerization efficiency of these systems and that the LED@405nm is more suitable for FRP of PEG-diacrylate.

Upon comparison of the polymerization efficiencies of the different PISs, the final acrylate function conversions and the polymerization rates, dyes 6 and 7 proved to be excellent candidates to promote the polymerization processes both in thin films and thick films, as well as with a LED@405nm and with a LED@375nm (e.g., the FCs of dye 7 were of 93% for thin films with a LED@405nm, of 96% for thick films with a LED@405nm, and 79% for thin films with a LED@375nm). Therefore, these two dyes were selected from the series of 18 dyes as representative structures and the LED@405nm was selected as the most appropriate light source for more detailed investigations concerning the mechanism.

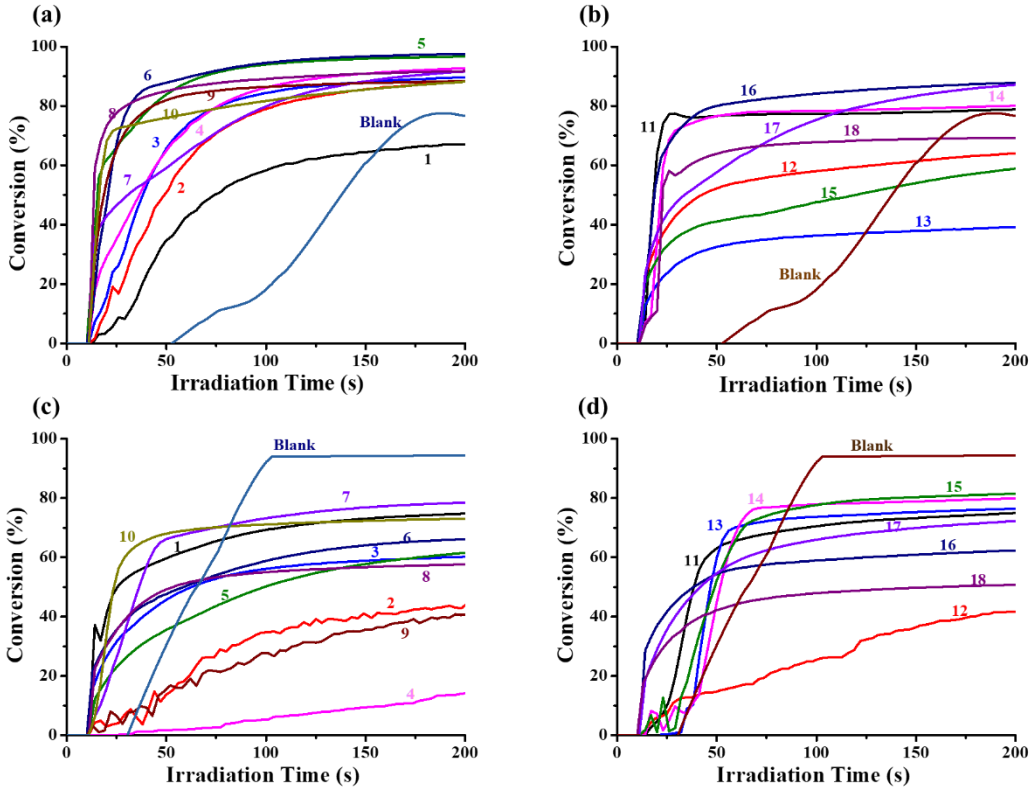

Figure 1. Photopolymerization profiles of PEG RS610 (conversion rate of C=C bonds vs irradiation time) initiated with the iodonium (Iod) salt and the amine (EDB) in laminate in the presence of dyes 1-18 for curves 1-10 (a) and 11-18 (b) upon exposure to a LED@405nm as well as for curves 1-10 (c) and 11-18 (d) upon exposure to a LED@375nm at the same weight ratio: dye:Iod:amine = 0.5%:1.5%:1.5%. The irradiation time starts at t =10 s (1 drops of formulation in 2pp films).

FCs of dyes-based PISs for FRP of PEG-diacrylate				
	FCs with the LED@405nm		FCs with the LED@375nm	
	Thin films (%)	Thick films (%)	Thin films (%)	Thick films (%)
1	67	88	75	-
2	88	90	44	-
3	90	98	60	-
4	93	42	14	-
5	97	61	62	-
6	98	93	66	-

7	92	96	79	-
8	92	51	58	42
9	88	78	41	35
10	88	27	73	-
11	79	-	78	-
12	64	-	47	-
13	40	-	79	-
14	80	-	82	-
15	60	26	84	6
16	88	28	66	14
17	87	21	76	9
18	70	-	54	-
Blank	76	93	94	95

"-" means it didn't be polymerized

Table 1 Summary of the FCs of monomers (PEG-diacrylate) under irradiation with a LED@405 nm and a LED@375 nm with the three-component photopolymerization systems based on dyes (0.5%, w/w), iodonium salt (Speedcure 938, 1.5%, w/w) and amine (EDB, 1.5%, w/w) in thin films and thick films.

3.2 Cationic Polymerizations (CP) Kinetics of EPOX.

As the ferrocene-based dyes (11-18) are mainly used to induce the polymerization of epoxy compounds, the different three-component systems (dyes/Iod/amine, 0.5 %/1.5% w/1.5%, w/w/w) were used as PISs for the CP of EPOX. The function conversions vs. irradiation time curves obtained using RT-FTIR are given in Figure 2 and the final conversions (FCs) of the epoxide functional groups of monomers are summarized in the Table 2. The three-compound PISs could provide good polymerization efficiencies in terms of final epoxy function conversions (FCs) with the irradiation of LED@ 405nm. Especially, all of them were capable to initiate a polymerization. In the same irradiation conditions, Iod and EDB alone were also tested

as blank control and proved to be poor PISs, characterized by their lower polymerization rates (the slope of the curve) and moderate function conversions (76%), highlighting the crucial role of the three-component systems for the overall performance. The trend of efficiency for the CP is not directly linked to their respective absorption properties (ε@405nm) that follow another trend (i.e. 6 > 3 > 7> 5 > blank > 2 > 4 > 1 > 8 >10 > 9 for the first series of dyes; 12 > 17 > blank > 13 > 11 > 14 > 15 >16 > 18 for the second series of dyes). Therefore, the polymerization ability of these dye-based PISs is also dependent on their photochemical reactivity with the iodonium salt and the amine as well as their ability to generate relevant radical cations ($dyes^{\bullet+}$) that can initiate the CP process. Interestingly, the two dyes 6 and 7 also proved to efficiently promote the photopolymerization of EPOX. Final reactive function conversions higher than 90% were attained within 50 s of irradiation. Remarkably, these two dyes have similar chemical structures, except that the substitution position of the methoxy group is different- the methoxy group is in the ortho position for dye 6, while for dye 7 this group is in the para position.

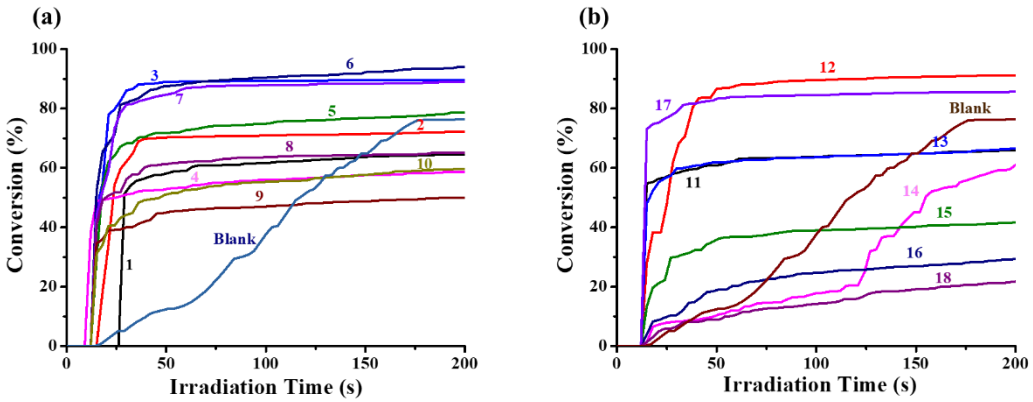

Figure 2. Photopolymerization profiles of EPOX (conversion rate of EPOX characteristic bonds vs irradiation time) initiated by iodonium (Iod) and amine (EDB) upon exposure to LED@405nm under air in the presence of dyes 1-18 for curves 1-10 (a) and 11-18 (b) at the same weight ratio: dye:Iod:amine = 0.5%:1.5%:1.5% in 1g EPOX. The irradiation time starts at t = 10 s (1 drops of formulations upon polished films).

FCs of dyes-based PISs for CP of EPOX					
Dyes	1	2	3	4	5
FCs (%)	78	97	64	28	98
Dyes	6	7	8	9	10
FCs (%)	64	83	63	75	25
Dyes	11	12	13	14	15
FCs (%)	55	68	65	21	61
Dyes	16	17	18	Blank	
FCs (%)	48	73	73	85	

Table 2 Summary of the FCs of monomers (EPOX) obtained upon irradiation with a LED@405 nm with the three-component photopolymerization systems based on dyes (0.5%, w/w), iodonium salt (Speedcure 938, 1.5%, w/w) and amine (EDB, 1.5%, w/w) upon polished films.

3.3 Free Radical Polymerization (FRP) Kinetics of PEG-diacrylate Initiated by Dyes 6 and 7 Based Two-Component PISs or Dyes alone as the PIs

To highlight the crucial role of the three-component systems for the overall performance, three other photoinitiating systems were investigated, namely i) dyes 6 or 7 / Iod (0.5%/1.5%, w/w) and dyes 6 or 7 /EDB (0.5%/1.5%, w/w) two-component PISs and ii) dyes 6 or 7 alone as PIs (0.5%, w/w) to initiate the FRP of PEG-diacrylate with the irradiation of a LED@405nm both in thin films and thick films. As depicted in the Figure 3, the samples containing only dyes 6 or 7 were not able to initiate the photopolymerization either in thick films or thin films. After the addition of amine, the samples could polymerize between thin films but the polymerization efficiency was lower than that of the three-component PIS (e.g. for the dyes/amine-based systems FCs $\leqslant$85%, for the dyes/Iod/amine based systems FCs$\geqslant$90%); in addition, all the samples weren't polymerized in the thick films (see Figure 3). Furthermore, samples based on the two-component dyes 6 or 7/Iod PISs can polymerize efficiently both in the thick

molds and thin films. High polymerization efficiencies could be observed for the dyes/Iod based systems (~ 95%) in thin films which was similar to that obtained with the three-component systems (dyes/Iod/amine, 93%-98%), while for the thick films, the polymerization profiles of these two dyes-based systems with the combination of Iod were significantly lower than those of the three-component systems (e.g. for the dyes/Iod based systems FCs≤80%, for the dyes/Iod/amine based systems FCs≥90%). The above results indicate that the photopolymerization efficiency can be improved when the amine or the iodonium salt were combined with the dyes, especially the best polymerization efficiency could be obtained when the three-component photoinitiating systems based on dyes/Iod/EDB were used as PISs.

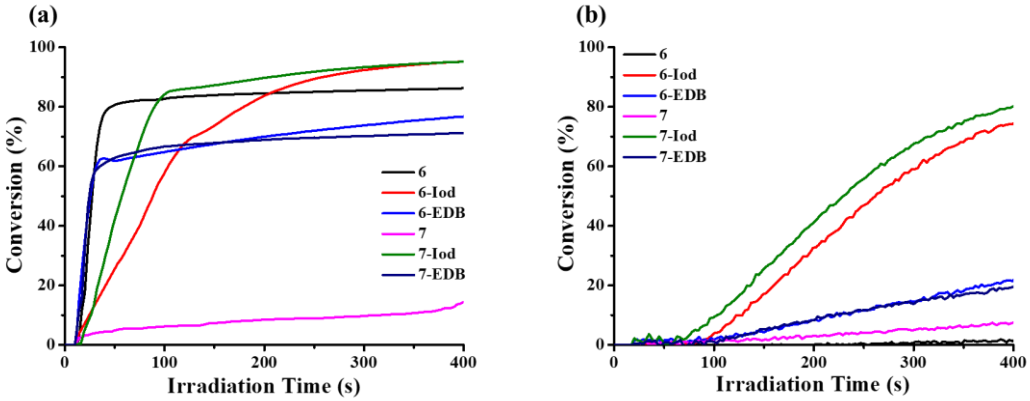

Figure 3. Photopolymerization profiles of PEG RS610 (conversion rate of C=C bonds vs irradiation time) initiated with 0.5% dye 6, 0.5% dye 6/1.5% Iod, 0.5% dye 6/1.5% EDB, 0.5% dye 7, 0.5% dye 7/1.5% Iod as well as 0.5% dye 7/1.5% EDB upon exposure to LED@405nm in laminate (a) in thin films and (b) in thick films. The irradiation time starts at t = 10 s.

FCs of dyes 6 and 7-based PISs for the FRP of PEG-diacrylate							
LED@405nm In thin films	**Dyes**	6	6-Iod	6-EDB	7	7-Iod	7-EDB
	FCs (%)	-	95	77	-	95	84
LED@405nm In thick films	**Dyes**	6	6-Iod	6-EDB	7	7-Iod	7-EDB
	FCs (%)	-	76	-	-	80	-

Table 3 Summary of the FCs of monomers (PEG-diacrylate) upon irradiation with a LED@405 nm initiated with 0.5% dye 6, 0.5% dye 6/1.5% Iod, 0.5% dye 6/1.5% EDB, 0.5% dye 7, 0.5% dye 7/1.5% Iod as well as 0.5% dye 7/1.5% EDB in laminate in thin films and thick films.

3.4. Generation of 3D Patterns with Dyes Containing Three-Component Photoinitiating Systems.

The FRP process of acrylates (PEG-diacrylate) could also be studied by its application in laser writing experiments under air using the dyes 6 and 7 based three-component PIS (dyes/Iod/amine, 1.5%/1.5%/1.5%, w/w/w) due to their high photosensitivity. As shown in Figure 4, the tridimensional patterns "**CTC**" could be fabricated successfully with an excellent spatial resolution upon irradiation with a laser emitting at 405 nm, in which the writing process with dye 7 was faster than with dye 6 because of its higher polymerization efficiencies in thick films, which is similar to the systems using well-established phosphine-oxides (TPO or TPOL) as benchmark photoinitiators. After that, further profilometric observation with a numerical optical microscope was used to characterize these letter patterns. All these results showed that writing with a remarkable spatial control was possible with the newly proposed photoinitiators by laser write experiments.

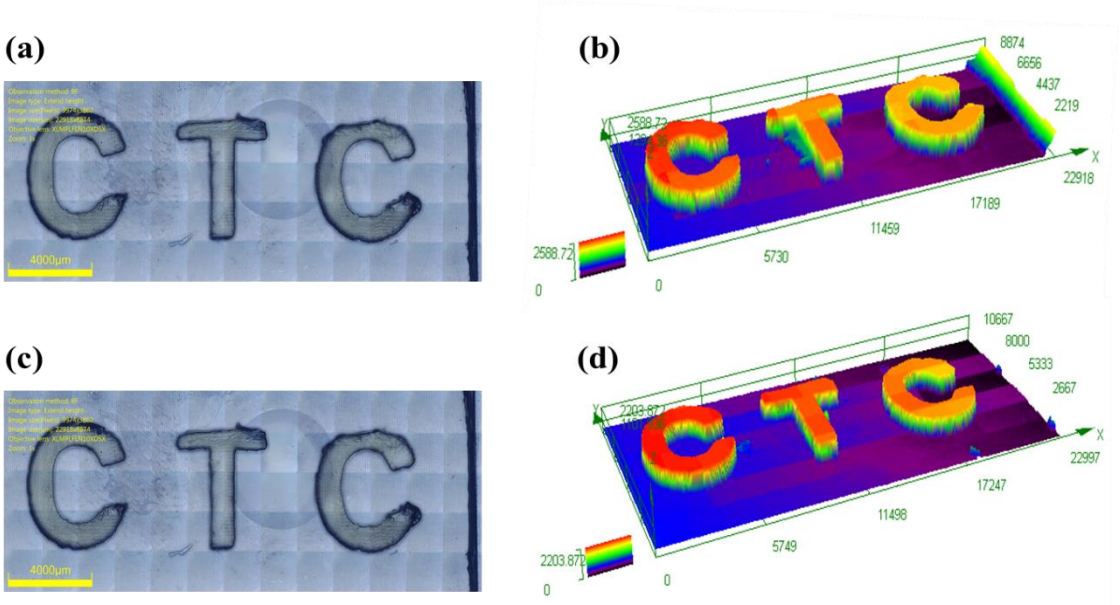

Figure 4. Laser writing experiments for FRP of PEG-diacrylate initiated by

dyes/Iod/EDB (1.5%/1.5%/1.5%, w/w/w) based three-component PISs. Characterization of the 3D patterns by numerical optical microscopy for top surface morphology (left) and 3-D overall appearance of color pattern (right): (a) (b) for dye 6; (c) (d) for dye 7.

*3.5 The Swelling of the "**T**" 3D Patterns Obtained by Laser Writing Experiments.*

The swelling ratio of the PEG-polymers - "**T**" 3D patterns - obtained using the dyes based three-component PISs were investigated by immersing the products in deionized water for 24 h to reach the swelling equilibrium. As shown in Figure 5a, the swelling ratio of the products obtained with dye 6 was about 46%, while for the dye 7 based patterns it was about 70%, owing to the higher extinction coefficients at the emission wavelength of the LED@405 nm and higher polymerization efficiencies in thick films for dye 7, which resulted in a higher degree of polymerization of dye 6 than for dye 7. After reaching swelling equilibrium, the "**T**" 3D patterns became bigger than the initial size (see in Figure 5b) and their volumes were increased about 160%~170% from their primary volume (see in Table 4). Then, after heating at 50°C for 0.5 hours, these 3D patterns could return to their original form, which indicates that the swelling of these 3D patterns and polymers is reversible.

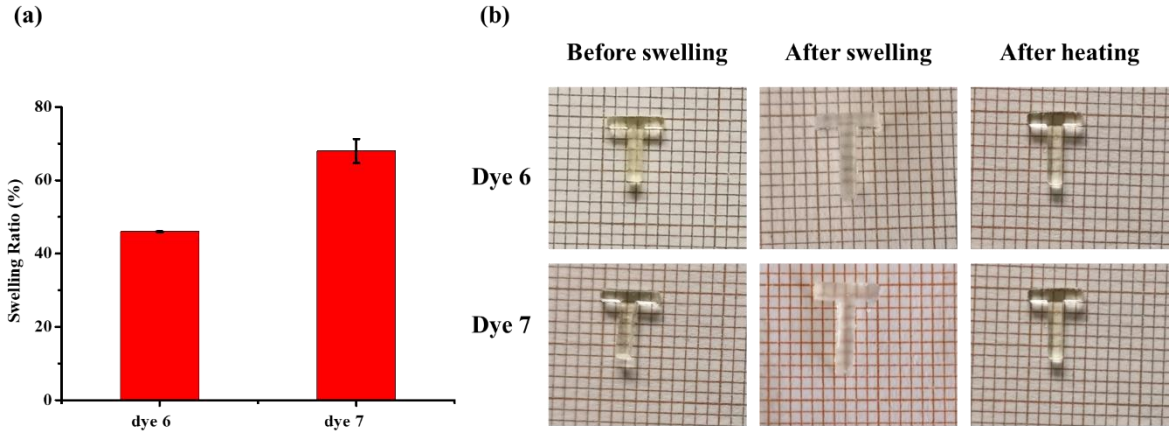

Figure 5. (a) the swelling ratio of PEG-polymer prepared using dyes 6 and 7 as photoinitiators; (b) the photos of the "**T**" 3D patterns based on PEG-polymers (obtained by laser write experiments using the dyes/Iod/EDB based three-component PIS) before water swelling, after water swelling for 24h and after heating for 0.5h to remove water.

	Dye 6	Dye 7
V_1 (mm^3)	19.49	21.46
V_2 (mm^3)	32.48	37.92
V_3 (mm^3)	19.89	20.40
R (%)	166.7%	176.7%

Table 4. The volumes of the "**T**" 3D pattern in the cycle: before swelling (V_1), equilibrium (V_2), water removal (V_3) as well as the increase ratio of volume after reaching swelling equilibrium (R).

3.6 Reversible Deformation: 4D Behavior of PEG-polymer via Thermoresponsive and/or Water-Responsive Induced Actuation

Hydrogels with a spatial control has been successfully formulated with the proposed PISs by laser writing experiments. Furthermore, a 4D behavior of PEG-polymer prepared with the proposed photoinitiators induced by thermoresponsive and/or water-responsive was also studied. Previous work has studied the effect of exposure time on the deformability of hydrogels prepared by the dye-based three-component PIS combined with PEG-diacrylate system [43]. In this work, we have further studied the impact of PEG-diacrylate monomers with different molecular weights on 4D behavior through the swelling and dehydration induced actuation. As shown in Figure 6a, we designed and obtained a cross-shaped object (length~58mm, width~47mm and height~1mm) with spatial resolution characteristics using PEG-diacrylate monomers with molecular weights about 400 and 610 under the same irradiation conditions. During the thermoresponsive and water-responsive shape-memory process, we observed that the cross prepared with PEG-diacrylate (Mw=610) achieved the maximum deformation during swelling and then returned to its original shape after dehydration whose structure remained complete. However, due to the poor toughness of the cross prepared with PEG-diacrylate (Mw=400), even though a certain degree of deformation can occur during swelling, it breaks during dehydration. Therefore, the cross formulated with PEG-diacrylate (Mw=610) was employed to

investigate the reversible deformation behavior via swelling and dehydration induced actuation. A cross was obtained by exposing the resin @405nm for 1 min (see Figure 6 (b)-1). After that, taking it into a water filled beaker, we observed that it began to deform as the water swollen, which caused the cross completely curled after swelling in water for 2 min (Figure 6 (b)-2 and SI Video 1). Subsequently, the cross was removed from water and heated at 80^{o}C to induce evaporation. Correspondingly, with the removal of the contained water, the curled cross flattened and recovered to its initial shape within 2 min (Figure 6 (b)-3 and SI Video 1). When the cross continued to dehydrate until 10 min, as shown in Figure 6 (b)-4, it curled up again. Furthermore, we removed the cross from 80^{o}C to room temperature for 10 min, the curled one gradually flattens out or even return to its original shape (see Figure 6 (b)-5). When the cross was swollen in water again for 1 min, it still deformed completely again as shown in Figure 6 (b)-6 and SI Video 2. After heating at 80 ^{o}C for 2 min, the curled cross partially restored to its primary shape (see Figure 6 (b)-7 and SI Video 2). The cross completely returned to its original shape after continuing the dehydration for 10 min, as shown in Figure 6 (b)-8. All these results demonstrated that the hydrogels initiated by the dyes/Iod/amine based novel PIS have a reversible deformation effect due to thermoresponsive and water-responsive processes, which corresponding to the molecular weights of PEG-diacrylate.

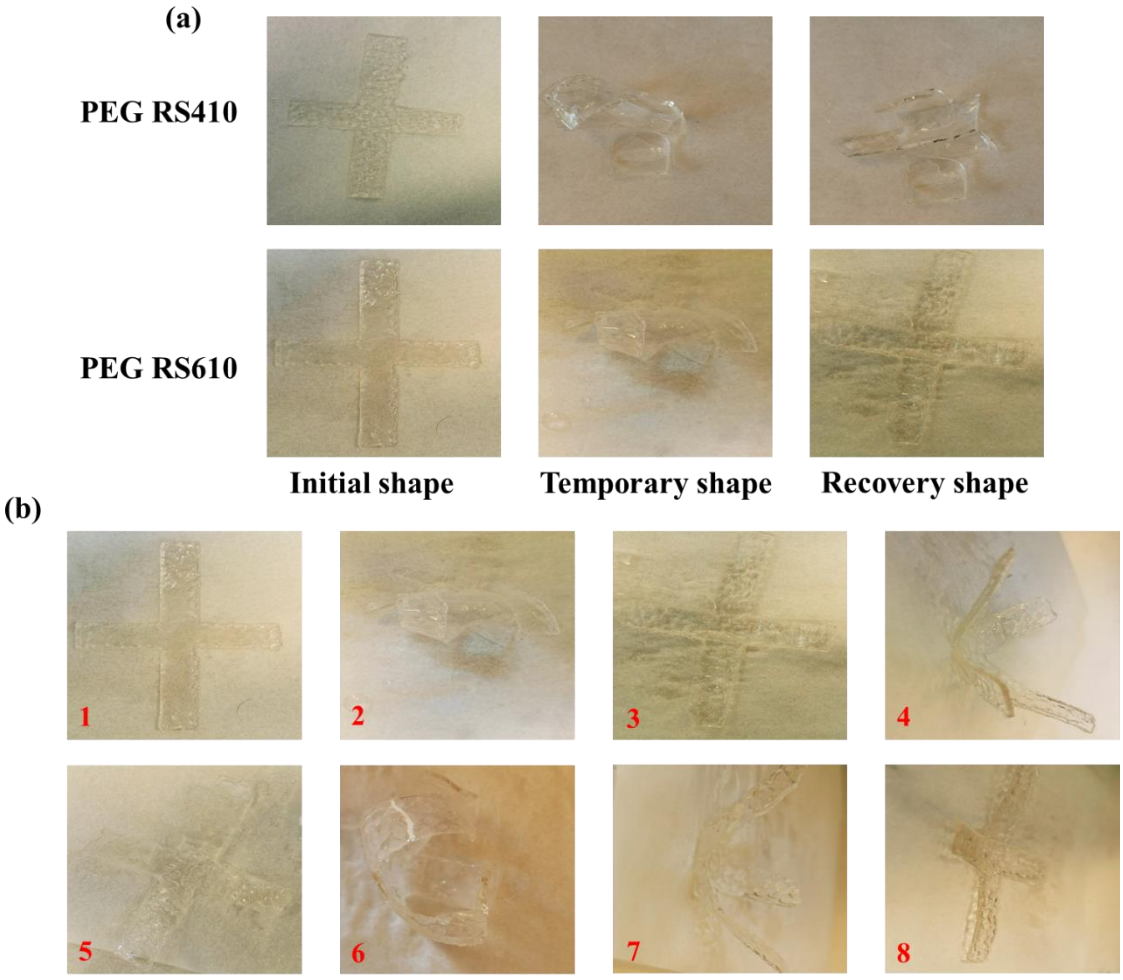

Figure 6. (a) Swelling and dehydration induced actuation of PEG-polymer with different molecular masses (Mw= 415/610) initiated by dye 6/Iod/amine irradiation with LED@405 nm; (b) Reversible deformation of PEG-polymer (Mw=610) initiated by dye 6/Iod/amine irradiation with LED@405 nm: (1) the cross of PEG-polymer after 1min light irradiation, (2) cross after water swelling for 1 min (see SI Video 1), (3) cross after 2 min of dehydration (heating at 100 ℃, see SI Video 1), (4) cross after 10 mins of dehydration (heating at 100 ℃), (5) cross after stay at room temperature for 10 mins, (6) cross after water swelling again for 1 min (see SI Video 2), (7) cross after 2 min of dehydration (heating at 80 ℃, see Video 2); (8) cross after 10 mins of dehydration (heating at 80 ℃).

4. Discussion

According to the results of the FRP, CP as well as 3D patterning and 4D behavior experiments, the two dyes (6 and 7) were chosen for the following mechanism studies.

For the photopolymerization process initiated with the three-component PIS, the chemical mechanisms as shown in Scheme 3 can be divided into two parts: (1) The dye acting as an electron donor and combined with an iodonium salt; (2) The dye acting as an electron acceptor and combined with an amine (EDB) that acts as an electron donor.

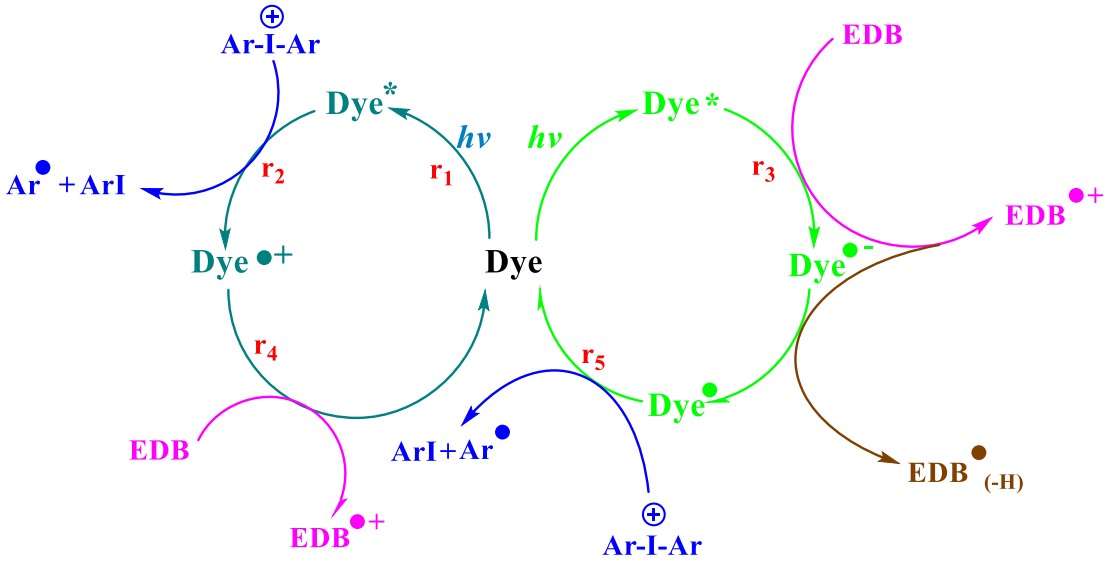

Scheme 3. Proposed photoinitiation mechanisms of dyes/Iod/amine initiating systems involving related radicals and cations generation.

4.1 Light Absorption Properties of the Dyes in Acetonitrile.

The UV-visible absorption spectra of the 18 different dyes in acetonitrile are presented in Figure 7, while their absorption maxima (λ_{max}) and extinction coefficients (ε_{max}) at λ_{max} and at the emission wavelength of the LED@405 nm ($\varepsilon_{@405\ nm}$) and LED@375 nm ($\varepsilon_{@375\ nm}$) are presented in Table S1. Except for dyes 8 and 9 whose maximum absorption peaks appeared at 400~410 nm, the maximum absorption wavelengths of the other dyes are lower than 380nm, thus ensuring a good overlap with the emission spectra of the LED@375 nm and the LED@405 nm used in this work. Furthermore, all the dyes exhibited high extinction coefficients (ε_{max} ~10^5 $M^{-1}cm^{-1}$) corresponding to π-π* electronic transitions that can be well observed in the molecular modeling results (depicted in the Figure 8).

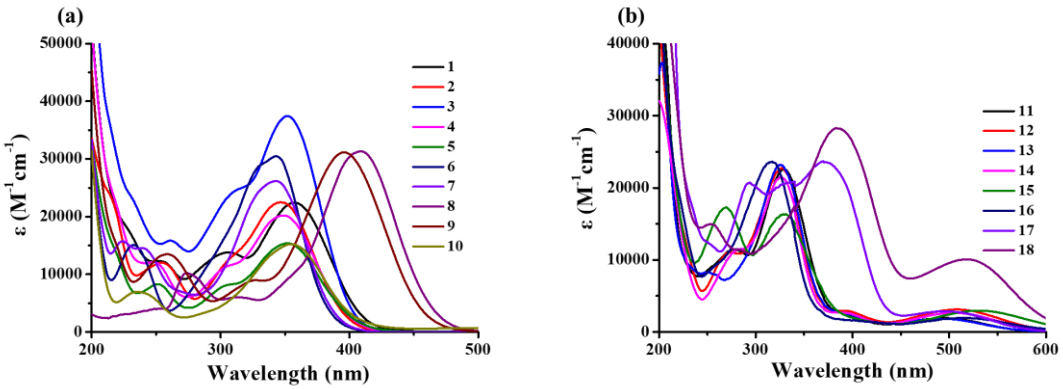

Figure 7. The UV-visible absorption spectra of dyes 1-10 (a) and 11-18 (b) in acetonitrile.

	HOMO	LUMO
(Dye6) 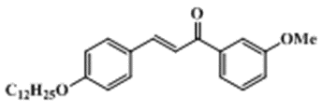	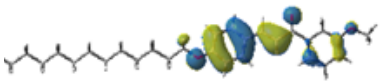	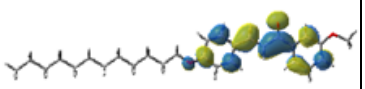
(Dye7) 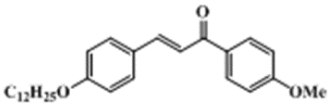	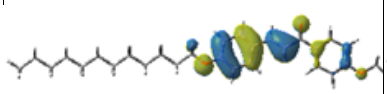	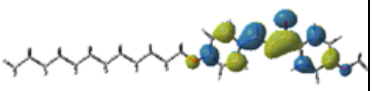

Figure 8. Contour plots of HOMOs and LUMOs for dyes 6 and 7; structures optimized at the B3LYP/6-31G* level of theory.

4.2 Steady-State Photolysis of Dyes 6 and 7 Characterized by UV-visible Absorption Spectroscopy

The steady-state photolysis for the dyes 6 and 7 in the presence of the iodonium salt and/or the amine were carried out in acetonitrile upon irradiation with a LED@405 nm. The effects of the iodonium salt and the amine on the photolysis of the two dyes are depicted in Figure 9, obvious photolysis and significant absorption decreases were observed for the dye-based three-component PIS(dye/Iod/amine) as well as the dyes based two-component PIS (dye/Iod or dye/amine). Interestingly, for the photolysis of dyes 6 or 7 alone as PI, the characteristic absorption peak at 340 nm decreased with the light irradiation, while a new absorption peak appearing at 270 nm increased of intensity. The photolysis of these two dyes based PIS are the same, which took 25 min because of their similar molar extinction coefficients and the photolysis in the first 5 min was faster than the latter 20 min. The above results show that the position of the methoxy substituent has no effect on the photolysis process.

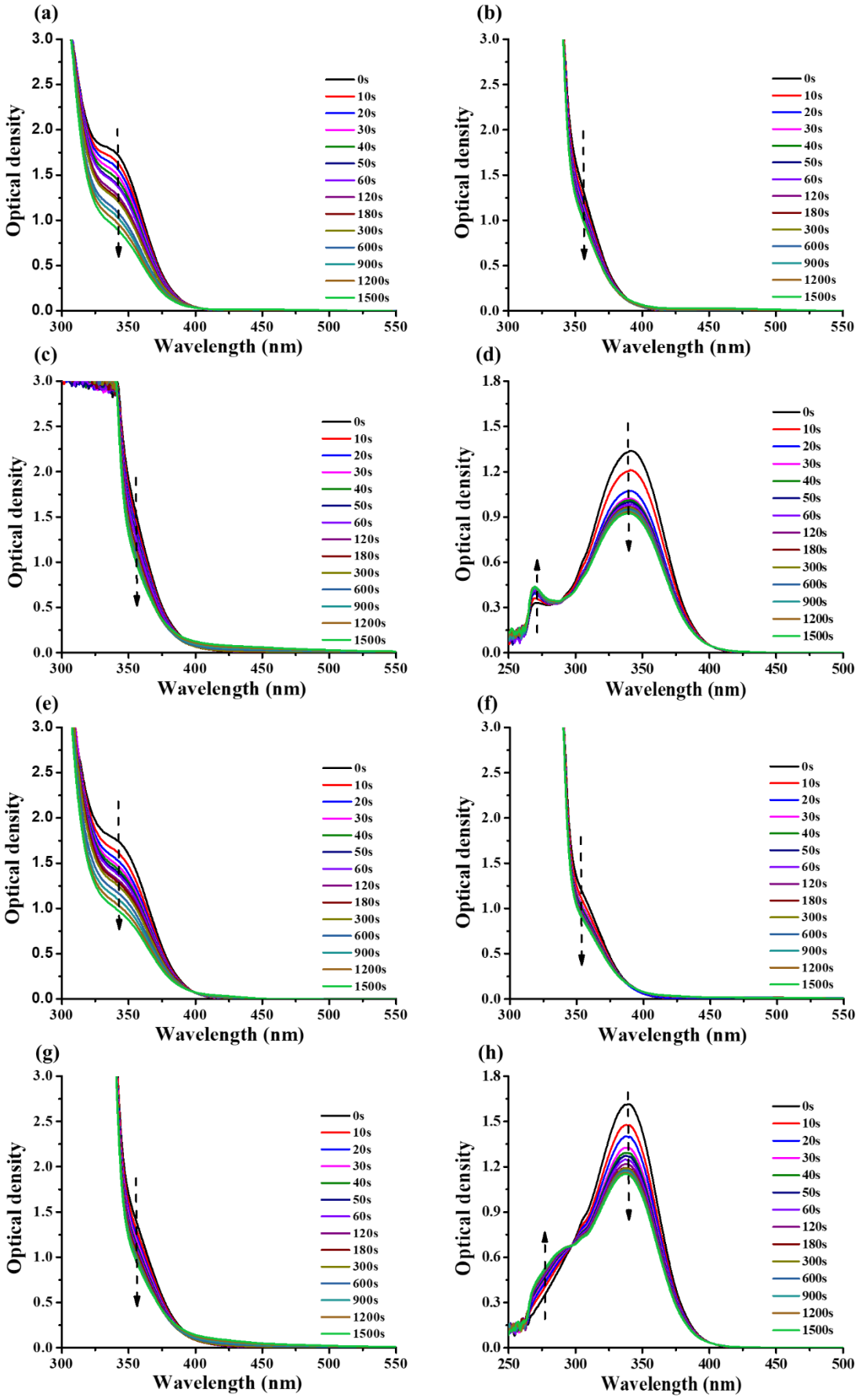
(a)
(b)
(c)
(d)
(e)
(f)
(g)
(h)
Optical density
Wavelength (nm)
0s
10s
20s
30s
40s
50s
60s
120s
180s
300s
600s
900s
1200s
1500s

Figure 9. Photolysis of (a) dye 6/Iod (5×10^{-5} M/0.01M); (b) dye 6/amine (5×10^{-5} M/0.01M); (c) dye 6/Iod/amine (5×10^{-5} M/0.01M/0.01 M); (d) dye 6 (5×10^{-5} M); (e) dye 7/Iod (5×10^{-5} M/0.01M); (f) dye 7/amine (5×10^{-5} M/0.01M); (g) dye 7/Iod/amine (5×10^{-5} M/0.01M/0.01 M); (h) dye 7 (5×10^{-5} M) upon exposure to a LED@405nm under air in the solvent of acetonitrile.

According to the photolysis presented above, we can summarize the consumption of the dyes vs. the irradiation time. The absorption changes detected in their UV-visible absorption spectra were examined both for the three-component PISs (chalcones/Iod/amine), the two-component PISs (chalcones/Iod or chalcones/amine) and the dyes alone as PI (illustrated in Figure S2) to investigate the chemical mechanisms. Clearly, the percentages of consumption profiles achieved for dyes 6 and 7 by the two-component PIS based on the dye/Iod combination were the highest, while the consumption of the dye in the dye/amine based two-component PIS was lower than that observed in the three-component systems (e.g. the consumption of dye 6 = 48% for dye 6/Iod *vs* 23% for dye 6/amine). During the same irradiation time, the consumption profiles for dyes 6 and 7 with the three-component PISs (dyes/Iod/amine) were quite close to that achieved when using the dyes alone as the PIs (e.g. the consumption of dye 6 = 31% for dye 6 alone *vs* 33% for dye 6/Iod/amine). It was proposed that the interactions of the dyes with Iod are much efficient than with the amine, and that the dye itself can also generate relevant free radicals when expose to the visible light to induce the FRP of PEG; in addition, $EDB^{\bullet+}$ radical can be formed by electron transfer from EDB, as an *N*-aromatic electron donor to dyes (r4), and the dyes can be regenerated from dye-$H^{\bullet}$ in the presence of an iodonium salt (r5), which decelerated the consumption of dyes 6 and 7.

4.3 Fluorescence Quenching and Cyclic voltammetry to Study the Electron Transfer Reaction for Dyes

The theoretical feasibility of the interaction between dye/Iod and dye/amine was studied by calculating the free energy changes (ΔG_{Iod} and $\Delta G_{EDB,}$ Table 5) of electron

transfer reactions. According to the equation (1) and equation (2), the oxidation potential E_{ox} and the reduction potential E_{red} for the dyes 6 and 7 was investigated through the Cyclic voltammetry (see in Figure S3), the first singlet excited state energy (E_{S1}) can be determined by the crossing point between the absorption of the UV-visible absorption spectra and the fluorescence spectra of these two dyes (e.g. E_{S1} = 3.28 eV for dye 6 and 3.30 eV for dye 7; Figure 10 and Table 5).

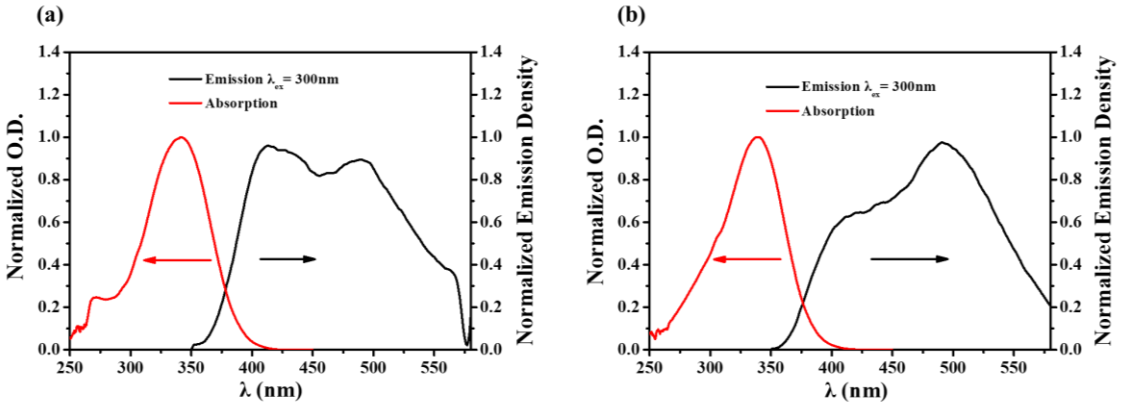

Figure 10. Singlet state energy determination in acetonitrile of (a) dye 6; (b) dye 7.

	Dye 6	Dye 7
E_{S1} (eV)	3.28	3.30
E_{T1} (eV)	2.18	2.21
E_{ox} (eV)	1.43	1.44
E_{red} (eV)	-0.01	-
ΔG_{S1}^{Iod}	-1.15	-1.16
ΔG_{S1}^{EDB}	-2.27	
ΔG_{T1}^{Iod}	*Must be added*	
ΔG_{T1}^{EDB}		

Table 5. Parameters characterizing the chemical mechanisms associated with dyes 6 and 7 in acetonitrile: singlet excited state energy (E_{S1}); E_{T1} extracted from molecular energy level calculations; oxidation potential (E_{ox}) and reduction potential (E_{red}) measured by Cyclic Voltammetry experiments as well as free energy change of singlet

electrode (ΔG_{S1}) and triplet electrode (ΔG_{T1}).

The fluorescence quenching experiments for dyes 6 and 7 were performed in acetonitrile to evaluate the efficiency of the dye/Iod and dye/amine interactions. As shown in Figure S4, without amine or iodonium, the luminescence of dyes 6 and 7 are very low. Interestingly, upon addition of Iod or amine into the solutions, an intense photoluminescence ascribed to the generation of photoproducts appeared, suggesting a good interaction between the dyes and the additives. After that, the fluorescence intensity of the solutions gradually decreased, even to zero, with the continual addition of Iod or amine, which indicated that they can be used as relatively good quenchers.

4.4 ESR Spin-Trapping Experiments

To better understand the interaction between dyes/Iod/amine, ESR spin-trapping experiments were carried out on dye 6/Iod, dye 6/amine and dye 6 solutions under N_2 using PBN as the spin trap agent.

Specifically, after light irradiation for 20s, three kinds of free radicals were detected in the dye 6/Iod solution through simulation (see in Figure 11 a and b): the PBN/aryl radical adduct is characterized by a_N = 14.4 and a_H = 2.2 G (fully matching to literature data [44]); oxygen centered radical ($ROO^{\bullet}$) is characterized by a_N = 13.4 and a_H = 1.7 G and the PBNox radical is characterized by a_N = 7.9 [45,46]. It suggested that the redox reaction (r2) between dye 6 and Iod takes place where Iod acts as an oxidizing agent leading to the formation of aryl radicals. Additionally, the dyes can also react with the PBN spin trap agent to generate the oxygen centered radical and PBNox.

Additional ESR-spin trapping experiments performed by irradiating the dye 6/amine solution for 50s as the interaction between dye and amine was weaker than that of the dyes with Iod. The results are presented in Figures 11c and d. Interestingly, a radical adduct corresponding to PBN/$ArNCH_3CH_2^{\bullet}$ adduct was detected and characterized by a_N = 14.4 and a_H = 2.1 G in agreement with literature data [47]. In addition, two other radicals were also detected, that were characterized by a_N = 14.0 and a_H = 5.2 G for the photolysed product from PBN and a_N = 7.9 for PBNox radical.

Finally, the ESR-spin trapping experiments were also carried out for dye 6/PBN solution with the light irradiation for 430s (see in Figure S5), the simulation gave four kinds of free radical generated in the dye 6/PBN solution: a_N = 14.0 and a_H = 5.2 G for the photolysed product from PBN, a_N = 13.3 and a_H = 1.6 G for oxygen centered radical, a_N = 14.2 and a_H = 2.0 G for the carbon centered radical and a_N = 7.9 for PBNox radical.

To assume that the dye in its excited state when react with PEG monomer, the polymerization of dye 6 in PEG-diacrylate was followed by ESR, and the results are shown in Figure S6. It's indicated that under the light irradiation, PEG-diacrylate can be induced to polymerize through the photolysis products of the dye itself or the adducts generated from the reaction of dyes with PEG-diacrylate.

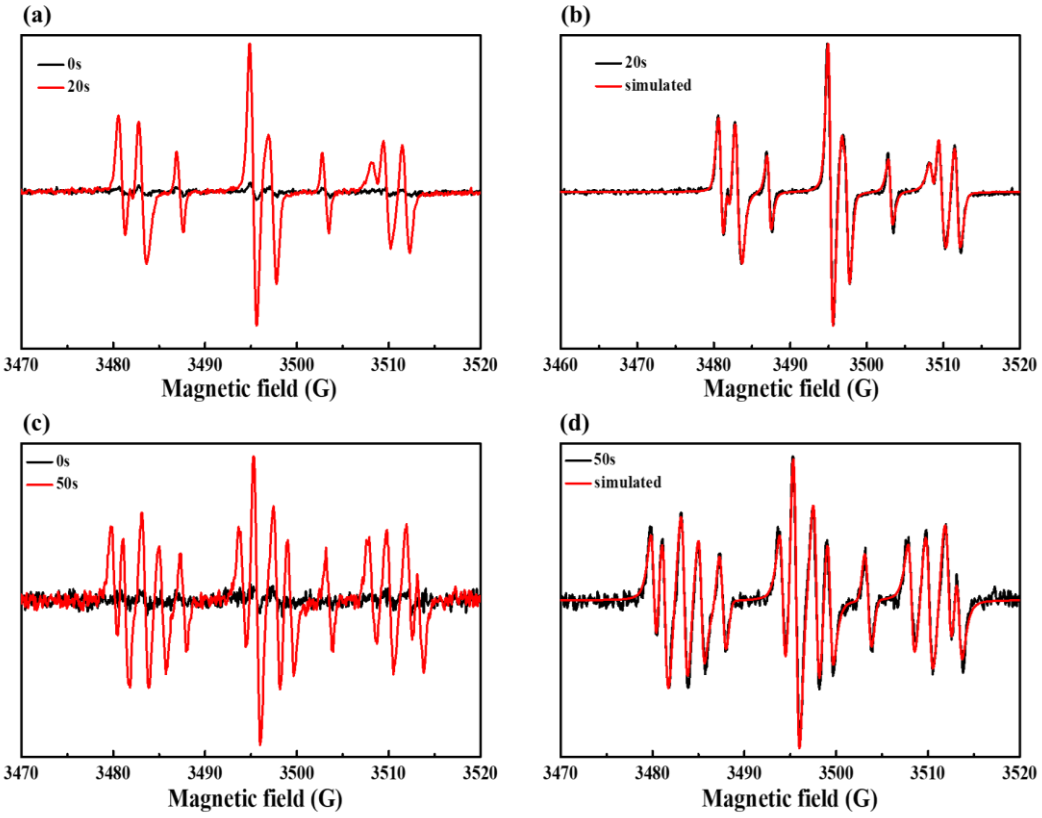

Figure 11. ESR spectra obtained from ESR-spin trapping experiment using PBN = 2 mg/mL (as spin trap agent); iodonium salt (Speedcure 938) = 12.6 mg/mL; amine (Speedcure EDB) = 12.6 mg/mL and dye 6 = 0.8 mg/mL in acetonitrile under N_2:(a) dye 6 /Iod Irradiation time = 20 s (red) and = 0 s (black) spectra; (b) dye 6 /Iod Irradiation time = 20 s (black) and simulated (red) spectra; (c) dye 6 /EDB Irradiation time = 50 s (red) and = 0 s (black) spectra; (d) dye 6 /EDB Irradiation time = 50 s (black)

and simulated (red) spectra.

5. Conclusions

In this work, 18 new dyes that can be divided into two distinct series were used for the elaboration of new photoinitiating systems capable of initiating high performance photopolymerizations. Specifically, two series of alkoxy based chalcones derivatives and ferrocene based-chalcones derivatives appeared as efficient photoinitiators for 405 nm and 375nm LED light induced photopolymerization accompanied with an iodonium salt and an amine. The results on FRP kinetics of monomer (PEG- diacrylate) and CP kinetics of monomer (EPOX) initiated by the new dye-contained photoinitiating systems were systematically investigated and dyes 6 and 7 were evaluated as the excellent photoinitiators. Moreover, the steady-state photolysis of dye-based photoinitiated systems was detected, and their proposed chemical mechanisms were discussed through the consumption curves of dyes. The calculation of free energy changes and ESR experiments confirmed the electron transfer between dyes, iodonium salts and amines in the photopolymerization process. It was also found that both good light absorption properties and excellent photochemical reactivities in the excited state processes (redox reactions) are required for the dyes to achieve an effective photoinitiation ability. Finally, good 3D patterns with remarkable spatial resolutions could be written using the newly proposed three-component PIS and the obtained PEG-polymer could exhibit an excellent thermal and water-responsive shape memory effects. This study contributes to improve the knowledge of photopolymerization carried out with LED@405nm by the development of new PISs comprising as its conjugation effect, which corresponds to different substituent groups (alkoxy or ferrocene). In addition, an environmentally friendly photocurable resin containing PEG-DA with different molecular masses as the monomers, dyes used as photoinitiators in conjunction with an iodonium salt as co-initiator and an amine as the electron donor were successful achieved with application to 3D and 4D printing processes. Furthermore, the swelling and dehydration induced shape-memory polymer network prepared by the above photocurable resin could be potentially applied for the

design of biomaterials. Future prospects will consist in…..

Author Contributions: Conceptualization, J.L., F.D., P.X.; methodology, J.L., F.D., P.X., C.H.; synthesis of dyes, F.D. and C.P.; software, B.G.; validation, all authors; formal analysis, J.L., F.D., P.X., C.H.; data curation, all authors; writing—original draft preparation, J.L., F.D., P.X., C.H.; writing—review and editing, all authors. All authors have read and agree to the published version of the manuscript.

Funding: China Scholarship Council (CSC) for C.H.; The Agence Nationale de la Recherche (ANR agency) through the PhD grant of Guillaume Noirbent (ANR-17-CE08-0054 VISICAT project). Aix Marseille University and the Centre National de la Recherche Scientifique (CNRS) are acknowledged for permanent fundings.

Acknowledgments: Authors wish to thank the Region Grand Est (France) for the grant "MIPPI-4D". This research project is supported by China Scholarship Council (CSC) (201906280059). P.X. acknowledges funding from the Australian Research Council (FT170100301). This work was granted access to the HPC resources of the Mesocentre of the University of Strasbourg.

Conflicts of Interest: The authors declare no conflict of interest.

References

1. Lalevee, J.; Fouassier, J.P. Photopolymerisation Initiating Systems. The Royal Society of Chemistry. London. 0,585, August 2018.

2. Ganster, B.; Fischer, U.K.; Moszner, N.; Liska, R. New photocleavable structures: Acylgermane-based photoinitiator for visible light curing. *Macromol. Rapid. Comm.* **2008**, *29*, 57-62.

3. Xiao, P.; Zhang, J.; Dumur, F.; Tehfe, M.A.; Morlet-Savary, F.; Graff, B.; Gigmes, D.; Fouassier, J.P.; Lalevée, J. Photoinitiating systems: recent progress in visible light induced cationic and radical photopolymerization reactions under soft conditions. *Prog.*

Polym. Sci. **2015**, *41*, 32-66.

4. Cook, W.D.; Chen, F. Enhanced visible radiation photopolymerization of dimethacrylates with the three component thioxanthone (CPTXO)-amine-iodonium salt system. *Polym. Chem.* **2015**, *6*, 1325-1338.

5. Xiao, P.; Wang, Y.; Dai, M.; Wu, G.; Shi, S.; Nie, J. Synthesis and photopolymerization kinetics of benzophenone piperazine one-component initiator. *Polym. Advan. Technol.* **2008**, *19*, 409-413.

6. Karaca, N.; Balta, D.K.; Ocal, N.; Arsu, N.J. Mechanistic studies of thioxanthone–carbazole as a one-component type II photoinitiator. *J. Lumin.* **2014**, *146*, 424–429.

7. Xu, J.; Boyer, C. Visible light photocatalytic thiol-ene reaction: An elegant approach for fast polymer post-functionalization and step-growth polymerization. *Macromolecules* **2015**, *48*, 520-529.

8. Kenning, N.S.; Ficek, B.A.; Hoppe, C.C.; Scranton, A.B. Spatial and temporal evolution of the photoinitiation rate for thick polymer systems illuminated by polychromatic light: Selection of efficient photoinitiators for LED or mercury lamps. *Polym. Int.* **2008**, *57*, 1134-1140.

9. Lalevée, J.; Blanchard, N.; Tehfe, M.A.; Peter, M.; Morlet-Savary, F.; Fouassier, J.P. A novel photopolymerization initiating system based on an iridium complex photocatalyst. *Macromol. Rapid Commun.* **2011**, *32*, 917-920.

10. Lalevée, J.; Allonas, X.; Fouassier, J.P. Addition of carbon-centered radicals to double bonds: Influence of the alkene structure. *J. Org. Chem.* **2005**, *70*, 814–819.

11. Michael L. Allegrezza, Zachary M. DeMartini, Alex J. Kloster, Zachary A. Digby, Dominik Konkolewicz. Visible and sunlight driven RAFT photopolymerization accelerated by amines: kinetics and mechanism. *Polym. Chem.* **2016**, *7*, 6626-6636.

12. Geérard, V.; Ay, E.; Morlet-Savary, F.; Graff, B.; Galopin, C.; Ogren, T.; Mutilangi, W.; Lalevée, J. Thermal and photochemical stability of anthocyanins from black carrot, grape juice, and purple sweet potato in model beverages in the presence of ascorbic acid. *J. Agric. Food Chem.* **2019**, *67*, 5647-5660.

13. Kaur, A., Singh, D. & Sud, D. A review on grafted, crosslinked and composites of biopolymer Xanthan gum for phasing out synthetic dyes and toxic metal ions from

aqueous solutions. *J. Polym. Res.* **2020**, *27*, 297.

14. Mahkam, M.; Kafshboran, H.R.; Nabati, M. Synthesis and characterization of novel colored polymers based on lawsone natural compound. *Des. Monomers. Polym.* **2014**, *17*, 784-794.

15. Mishra, A.; Daswal, S. Curcumin, a natural colorant as initiator for photopolymerization of styrene: kinetics and mechanism. *Colloid. Polym. Sci.* **2007**, *285*, 1109-1111.

16. Fouassier, J.P.; Morlet-Savary, F.; Lalevée, J.; Allonas, X.; Ley, C. Dyes as photoinitiators or photosensitizers of polymerization reactions. *Materials,* **2010**, *3*, 5130-5142.

17. Zhou, T.F.; Ma, X.Y.; Han, W.X.; Guo, X.P.; Gu, R.Q.; Yu, L.J.; Li, J.; Zhao, Y.M.; Wang, T.; D-D-A dyes with phenothiazine-carbazole/triphenylamine as double donors in photopolymerization under 455 nm and 532 nm laser beams. *Polym. Chem,* **2016**, *7*, 5039-5049.

18. Liu, C.; Qin, H.; Mather, P.T. Review of progress in shape-memory polymers. *J. Mater. Chem.,* **2007**, *17*, 1543-1558.

19. Kim, B.S.; Lee, S.H.; Furukawa, F. Handbook of Condensation Thermoplastic Elastomers. Fakirov, S. eds. Wiley-VCH, Weinheim, 521-566, **2005**

20. Lendlein, A.; Langer, R. Biodegradable, elastic shape-memory polymers for potential biomedical applications. Science. **2002**, *296*, 1673-1676.

21. Ratna, D.; Karger-Kocsis, J. Recent advances in shape memory polymers and composites: a review. *J. Mater. Sci.* **2008**, *43*, 254-269.

22. Liu, Y.; Lv, H.; Lan, X.; Leng, J.; Du, S. Review of electro-active shape-memory polymer composite. *Compos. Sci. Technol.* **2009**, *69*, 2064-2068.

23. Behl, M.; Razzaq, M.Y.; Lendlein, A. Multifunctional shape-memory polymers. *Adv. Mater.* **2010**, *22*, 3388-3410.

24. Skákalová, V.; Lukeš, V.; Breza, M. Shape memory effect of dehydrochlorinated crosslinked poly (vinyl chloride). *Macromol. Chem. Phys.* **1997**, *198*, 3161-3172.

25. Lin, J.R.; Chen, L.W. Study on shape-memory behavior of polyether-based polyurethanes. I. Influence of the hard-segment content. *J. Appl. Polym. Sci.* **1998**, *69*,

1563.

26. Jiang, H.Y.; Kelch, S.; Lendlein, A. Polymers move in response to light. *Adv. Mater.* **2006**, *18*, 1471-1475.

27. Cho, J.W.; Kim, J.W.; Jung, Y.C.; Goo, N.S. Electroactive shape-memory polyurethane composites incorporating carbon nanotubes. *Macromol. Rapid Comm.* **2005**, *26*, 412-416.

28. Mohr, R.; Kratz, K.; Weigel, T.; Lucka-Gabor, M; Moneke, M.; Lendlein, A. Initiation of shape-memory effect by inductive heating of magnetic nanoparticles in thermoplastic polymers. *Proc. Natl. Acad. Sci. USA* **2006**, *103*, 3540-3545.

29. Huang, W.M.; Yang, B. Water-driven programmable polyurethane shape memory polymer: demonstration and mechanism. *Appl. Phys. Lett.* **2005**, *86*, 114105.

30. Chen, S.; Hu, J.; Zhuo, H. Study on the moisture absorption of pyridine containing polyurethane for moisture-responsive shape memory effects. *J. Mater. Sci.* **2011**, *46*, 6581-6588.

31. Lendlein, A.; Kelch, S. Shape-memory polymers. *Angew. Chem. Int. Ed.* **2002,** *17,* 1973-2208.

32. Hu J.L.; Zhu, Y.; Huang, H.H.; Lu, J. Recent advances in shape–memory polymers: Structure, mechanism, functionality, modeling and applications. *Prog. Polym. Sci.* **2012**, *37*, 1720-1763.

33. Sofla, A.Y.N.; Elzey, D.M.; Wadley, H.N.G. Two-way antagonistic shape actuation based on the one-way shape memory effect. *J. Intell. Mater. Sys. Struct.* **2008**,*19*, 1017-1027.

34. Nechifor, M. Novel Chalcone-based Aromatic Polyamides: Synthesis, Characterization, and Properties. *Des. Monomers. Polym*. **2016**, *19*, 161-171.

35. Urano, T.; Nagao, T.; Takada, A.; Itoh, H. Photosensitization mechanisms in photopolymer coating film containing photoinitiators sensitized by aminochalcone-type dye for computer-to-photopolymer plate. *Polym. Adv. Technol.* **1999**, *10*, 244-250.

36. Ohto, N.; Niki, E.; Kamiya, Y. Study of autoxidation by spin trapping. Spin trapping of peroxyl radicals by phenyl N-t-butyl nitrone. *J. Chem. Soc. Perkin Trans.* **1977**, *13*, 1770–1774.

37. Romanczyk, P.P.; Kurek, S.S. The reduction potential of diphenyliodonium polymerisation photoinitiator is not −0.2 V vs. SCE. a computational study. *Electrochim. Acta*. **2017**, *225*, 482–485.

38. Pigot, C.; Noirbent, G.; Bui, T.T.; P é ralta, S.; Gigmes, D.; Nechab, M.; Dumur, F. Push-pull chromophores based on the naphthalene scaffold: potential candidates for optoelectronic applications. *Materials* **2019**, *12*, 1342.

39. Rehm, D.; Weller, A. Kinetics of fluorescence quenching by electron and H-atom transfer. *Isr. J. Chem.* **1970**, *8*, 259–271.

40. Scherzer, T. Real-time FTIR-ATR spectroscopy of photopolymerization reactions. *Macromol. Symp.* **2002**, *184*, 79-98.

41. Guvendiren, M.; Burdick, J.A.; Yang, S. Kinetic study of swelling-induced surface pattern formation and ordering in hydrogel films with depth-wise crosslinking gradient. *Soft. Matter.* **2010***, 6,* 2044-2049.

42. Chen, H.; Noirbent, G.; Sun, K.; Brunel, D.; Gigmes, D.; Morlet-Savary, F.; Zhang, Y.J.; Liu, S.H.; Xiao, P.; Dumur, F.; Lalevée, J. Photoinitiators derived from natural product scaffolds: monochalcones in three-component photoinitiating systems and their applications in 3D printing. *Polym. Chem.* 2020, 11, 4647-4659.

43. Chen, H.; Bonfiglio, A.; Morlet-Savary, F.; Matteo Mauro, M.; Lalevée, L. Rhenium(I) N-heterocyclic carbene Complexes in Photoinitiating Systems for Polymerization Upon Visible Light: Development of photosensitive resins for 3D and 4D printing applications. (under review)

44. Haire, L.D.; Krygsman, P.H.; Janzen, E.G.; Oehler, U.M. Correlation of radical structure with EPR spin adduct parameters: Utility of the proton, carbon-13, and nitrogen-14 hyperfine splitting constants of aminoxyl adducts of PBN-nitronyl- 13 C for three-parameter scatter plots. *J. Org. Chem.* **1988**, *53*, 4535-4542.

45. Alexander Halpern. Spin-trapping Study of the Radiolysis of CCl. *J. Chem. Soc., Faraday Trans.* **1987**,*83*, 219-224.

46. Jenkins, C.A.; Murphy, D.M.; Rowlands, C.R.; Egerton, T.A. EPR study of spin-trapped free radical intermediates formed in the heterogeneously-assisted photodecomposition of acetaldehyde. *J. Chem. Soc., Perkin Trans.* **1997**, *2*, 2479-2485.

47. Sun, K.; Xu, Y.Y.; Dumur, F.; Morlet-Savary, F.; Chen, H.; Dietlin, C.; Graff, B.; Lalevee, J.; Xiao, P. In silico rational design by molecular modeling of new ketones as photoinitiators in three-component photoinitiating systems: application in 3D printing. *Polym. Chem.,* **2020**, *11*, 2230-2242.

Supplementary Information

Photopolymerization and 3D/4D Applications Using Newly Developed Dyes: alkoxy and ferrocene based chalcone derivatives in Three-Component Systems

Hong Chen [a,b], Guillaume Noirbent [c], Yijun Zhang [a,b], Ke Sun [a,b], Shaohui Liu [a,b], Damien Brunel [c], Didier Gigmes [c], Bernadette Graff [a,b], Fabrice Morlet-Savary [a,b], Pu Xiao *[d], Frédéric Dumur * [c], Jacques Lalevée * [a,b]

[a] Université de Haute-Alsace, CNRS, IS2M UMR 7361, F-68100 Mulhouse, France

[b] Université de Strasbourg, France

[c] Aix Marseille University, CNRS, ICR UMR 7273, F-13397 Marseille, France; frederic.dumur@univ-amu.fr

[d] Research School of Chemistry, Australian National University, Canberra, ACT 2601, Australia; pu.xiao@anu.edu.au

* Corresponding author: jacques.lalevee@uha.fr (J. L.), frederic.dumur@univ-amu.fr (F. D.); pu.xiao@anu.edu.au (P. X.).

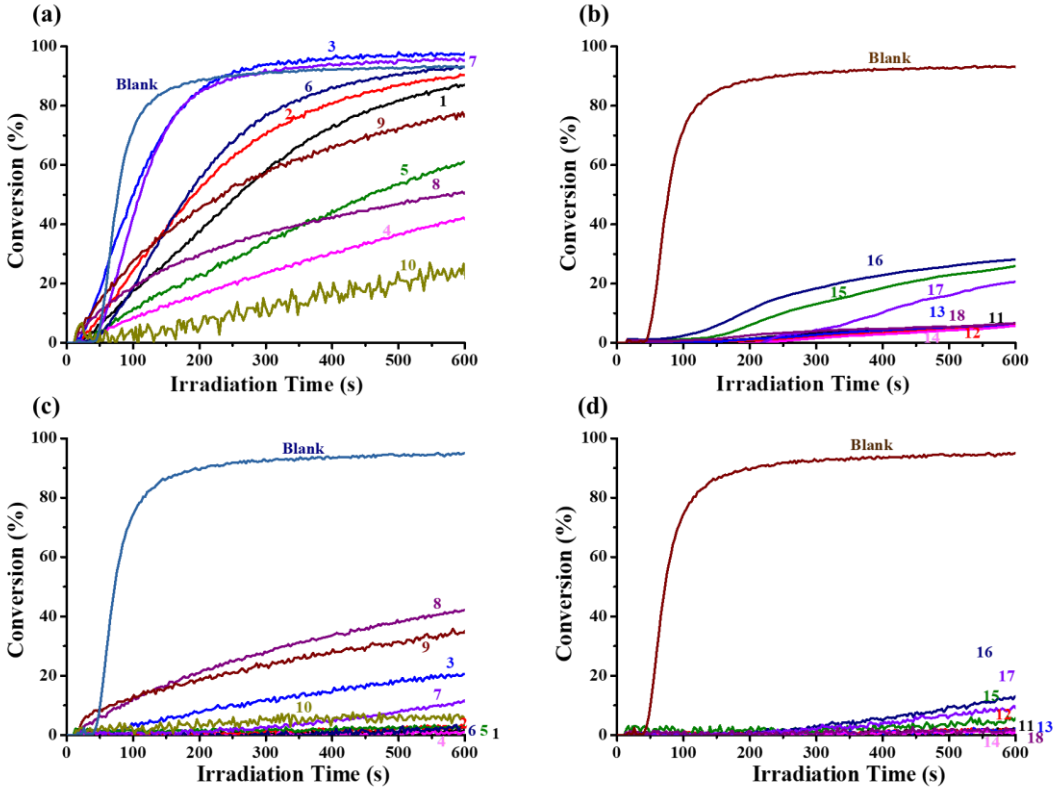

Figure S1. Photopolymerization profiles of PEG RS610 (conversion rate of C=C bonds vs irradiation time) initiated by iodonium (Iod) and amine (EDB) in laminate in the presence of dyes 1-18 for curves 1-10 (a) and 11-18 (b) upon exposure to LED@405nm as well as for curves 1-10 (c) and 11-18 (d) upon exposure to LED@375nm at the same weight ratio: dye:Iod:amine = 0.5%:1.5%:1.5% in 1g PEG. The irradiation time starts at t=10s (5 drops of formulation in thick film).

DYEs	$\lambda_{max\ (nm)}$	ε_{max} ($M^{-1}\ cm^{-1}$)	$\varepsilon_{@405nm}$ ($M^{-1}\ cm^{-1}$)	$\varepsilon_{@375nm}$ ($M^{-1}\ cm^{-1}$)
1	357	22 440	4090	18 030
2	349	22 520	1400	11 860
3	351	37 430	2840	24 200
4	349	20 270	1870	11 700
5	350	15 440	2040	10 090
6	341	31 100	480	8080
7	341	26 400	630	9400

8	411	31 370	31 100	16 960
9	396	31 180	29 660	24 660
10	355	15 200	2540	11 180
11	329	22 590	1970	3700
12	328	22 760	2250	3200
13	327	23 170	2130	3290
14	326	21 490	2230	2840
15	331	16 350	1810	4360
16	317	23 620	1550	2160
17	340	20 840	15 340	23 480
18	384	28 260	24 870	27 420

Table S1 Light absorption properties of dyes 1-18 in acetonitrile: maximum absorption wavelengths λ_{max}; extinction coefficients at λ_{max} (ε_{max}) and extinction coefficients at the emission wavelength of the LED@405 nm ($\varepsilon_{@405nm}$) and the LED@375 nm ($\varepsilon_{@375nm}$).

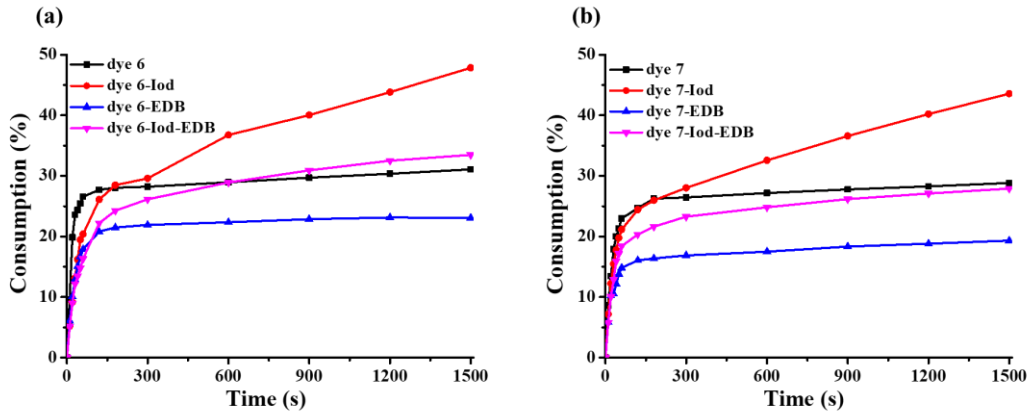

Figure S2 Consumption of (a) dye 6 and (b) dye 7 during the photolysis experiments.

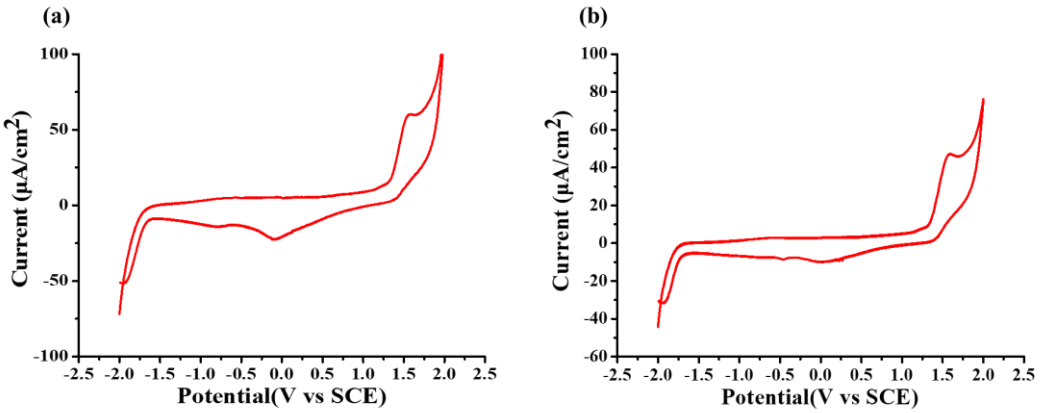

Figure S3. Cyclic voltammetry of electrochemical reactions of dyes 6 and 7 in acetonitrile solvent against saturated calomel electrode (SCE) under nitrogen saturated solution: (a) dye 6; (b) dye 7.

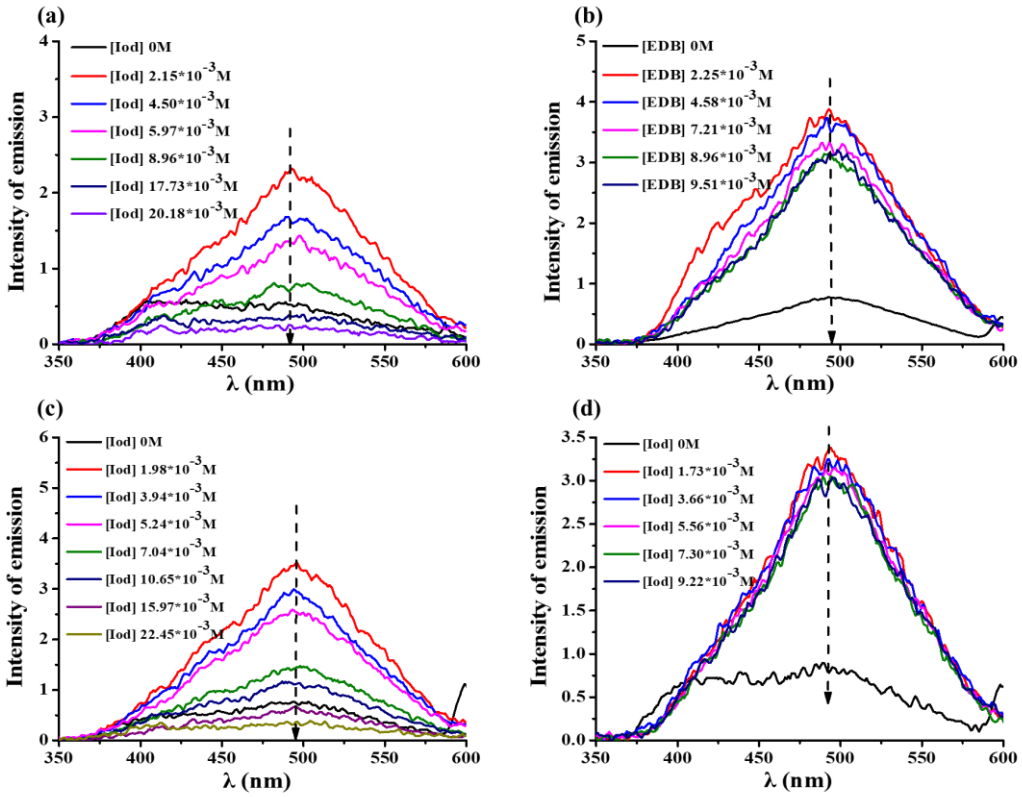

Figure S4. Fluorescence quenching of (a) dye 6 by iodonium salt (Speedcure 938); (b) dye 6 by amine (EDB); (c) dye 7 by iodonium salt (Speedcure 938); (d) dye 7 by amine (EDB).

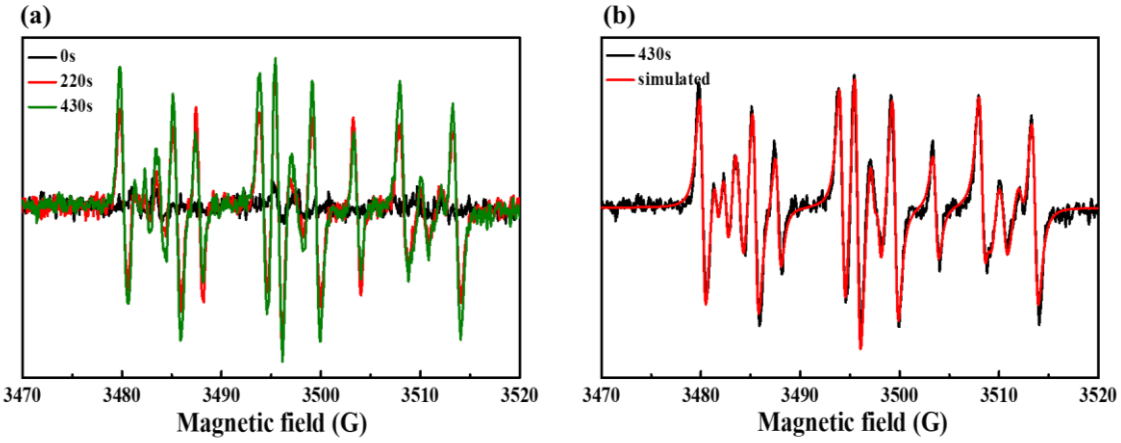

Figure S5. ESR spectra obtained from ESR-spin trapping experiment using PBN = 2 mg/mL (as spin trap agent) and dye 6 = 0.8 mg/mL in acetonitrile under N2: (a) dye 6 Irradiation time = 430s (green) 220 s (red) and = 0 s (black) spectra; (b) dye 6 Irradiation time = 430 s (black) and simulated (red) spectra.

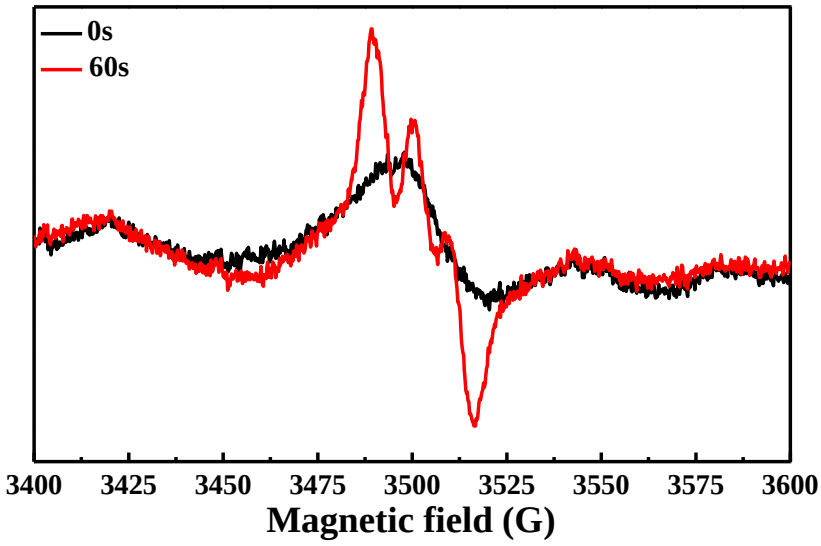

Figure S6. EPR spectra obtained from the polymerization of dye 6 in PEG-diacrylate (0.5%, w/w).

All reagents and solvents were purchased from Aldrich or Alfa Aesar and used as received without further purification. Mass spectroscopy was performed by the Spectropole of Aix-Marseille University. ESI mass spectral analyses were recorded with a 3200 QTRAP (Applied Biosystems SCIEX) mass spectrometer. The HRMS

mass spectral analysis was performed with a QStar Elite (Applied Biosystems SCIEX) mass spectrometer. Elemental analyses were recorded with a Thermo Finnigan EA 1112 elemental analysis apparatus driven by the Eager 300 software. ^{1}H and ^{13}C NMR spectra were determined at room temperature in 5 mm o.d. tubes on a Bruker Avance 400 spectrometer of the Spectropole: ^{1}H (400 MHz) and ^{13}C (100 MHz). The ^{1}H chemical shifts were referenced to the solvent peaks DMSO (2.49 ppm), $CDCl_3$ (7.26 ppm) and the ^{13}C chemical shifts were referenced to the solvent peak DMSO (49.5 ppm), $CDCl_3$ (77.0 ppm). All photoinitiators were prepared with analytical purity up to accepted standards for new organic compounds (>98%) which was checked by high field NMR analysis.

Synthesis of 3-(2,4-dibutoxyphenyl)-1-(4-methoxyphenyl)prop-2-en-1-one **1**

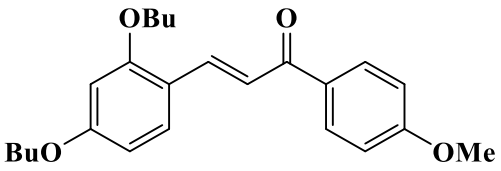

2,4-Dibutoxybenzaldehyde (5.00 g, 20 mmol, M = 250.34 g/mol) and 4'-methoxy-acetophenone (3.00 g, 20 mmol, M = 150.18 g/mol) were dissolved in ethanol (200 mL). During the reaction, a precipitate formed. It was filtered off and washed with a minimum of ethanol. The solid was dissolved in DCM and the solution dried over magnesium sulfate. The solution was filtered on a plug of silicagel to remove the excess KOH and concentrated under reduced pressure. It was isolated as a light yellow solid (6.20 g, 81% yield). ^{1}H NMR ($CDCl_3$) δ : 0.99 (t, 3H, J = 7.5 Hz), 1.01 (t, 3H, J = 7.5 Hz), 1.46-1.67 (m, 4H), 1.78 (qt, 2H, J = 6.9 Hz), 1.88 (qt, 2H, J = 6.4 Hz), 3.88 (s, 3H), 4.00 (t, 2H, J = 7.1 Hz), 4.04 (t, 2H, J = 7.1 Hz), 6.46-6.52 (m, 2H), 6.96 (d, 2H, J = 8.9 Hz), 7.52 (d,1H, J = 8.5 Hz), 7.65 (d, 1H, J = 15.7 Hz), 7.98-8.03 (m, 3H); ^{13}C NMR ($CDCl_3$) δ : 13.8, 13.9, 19.2, 19.5, 31.2, 31.3, 55.4, 67.9, 68.2, 99.6, 105.8, 113.7, 117.1, 120.2, 130.6, 131.7, 131.8, 140.3, 160.0, 162.4, 163.0, 189.5; HRMS (ESI MS) m/z: theor: 382.2144 found: 382.2148 ($M^{+\cdot}$ detected)

Synthesis of 3-(3,4-dibutoxyphenyl)-1-(2-methoxyphenyl)prop-2-en-1-one **2**

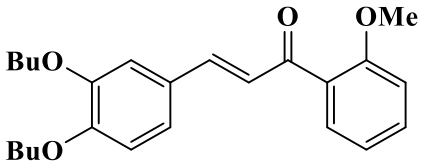

3,4-Dibutoxybenzaldehyde (5.00 g, 20 mmol, M = 250.34 g/mol) and 2'-methoxyacetophenone (3.00 g, 20 mmol, M = 150.18 g/mol) were dissolved in ethanol (200 mL). The solution was cooled into ice and aq. KOH 40% (20 mL) was added. The solution was stirred at room temperature overnight. It was filtered off and washed with a minimum of ethanol. The solid was dissolved in DCM and the solution dried over magnesium sulfate. The solution was filtered on a plug of silicagel to remove the excess KOH and concentrated under reduced pressure. It was isolated as a light yellow solid (6.43 g, 84% yield). ^{1}H NMR ($CDCl_3$) δ : 1.13 (t, 3H, J = 7.4 Hz), 1.14 (t, 3H, J = 7.4 Hz), 1.59-1.72 (m, 4H), 1.91-2.01 (m, 4H), 4.03 (s, 3H), 4.17 (qt, 2H, J = 6.6 Hz), 4.18 (m, 2H, J = 6.6 Hz), 7.01 (d, 1H, J = 8.8 Hz), 7.14 (d, 1H, J = 7.6 Hz), 7.18 (td, 1H, J = 7.5 Hz, J = 0.9 Hz), 7.27-7.29 (m, 1H), 7.38 (d, 1H, J = 15.8 Hz), 7.57-7.62 (m, 2H), 7.66 (d, 1H, J = 15.8 Hz), 7.71 (dd, 1H, J = 7.5 Hz, J = 1.8 Hz); ^{13}C NMR ($CDCl_3$) δ : 13.8, 13.9, 19.2, 19.3, 31.2, 31.3, 55.8, 68.8, 69.1, 111.6, 113.0, 113.1, 120.7, 123.0, 125.1, 127.9, 129.7, 130.1, 132.4, 144.1, 149.2, 151.6, 157.9, 193.4; HRMS (ESI MS) m/z: theor: 382.2144 found: 382.2147 ($M^{+\cdot}$ detected)

Synthesis of 3-(3,4-dibutoxyphenyl)-1-(4-methoxyphenyl)prop-2-en-1-one **3**

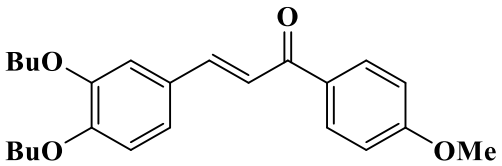

3,4-Dibutoxybenzaldehyde (5.00 g, 20 mmol, M = 250.34 g/mol) and 4'-methoxy-acetophenone (3.00 g, 20 mmol, M = 150.18 g/mol) were dissolved in ethanol (200 mL). The solution was cooled into ice and aq. KOH 40% (20 mL) was added and the solution was stirred at room temperature overnight. During the reaction, a precipitate formed. It was filtered off and washed with a minimum of ethanol. The solid was dissolved in

DCM and the solution dried over magnesium sulfate. The solution was filtered on a plug of silicagel to remove the excess KOH and concentrated under reduced pressure. It was isolated as a light yellow solid (5.74 g, 75% yield). ^{1}H NMR ($CDCl_3$) δ : 0.98 (t, 3H, J = 7.4 Hz), 1.00 (t, 3H, J = 7.4 Hz), 1.47-1.57 (m, 4H), 1.77-1.88 (m, 4H), 3.88 (s, 3H), 4.04 (t, 2H, J = 6.6 Hz), 4.06 (t, 2H, J = 6.6 Hz), 6.88 (d, 1H, J = 8.0 Hz), 6.97 (d, 2H, J = 8.9 Hz), 7.18-7.21 (m, 2H), 7.38 (d, 1H, J = 15.5 Hz), 7.74 (d, 1H, J = 15.5 Hz), 8.03 (d, 2H, J = 8.9 Hz); ^{13}C NMR ($CDCl_3$) δ : 13.8, 13.9, 19.2, 19.3, 31.2, 31.3? 55.5, 68.8, 69.2, 113.0, 113.1, 113.8, 119.6, 123.0, 128.0, 130.7, 131.4, 144.3, 149.2, 151.6, 163.2, 188.8; HRMS (ESI MS) m/z: theor: 382.2144 found: 382.2140 ($M^{+\cdot}$ detected)

Synthesis of 3-(2,4-*bis*(allyloxy)phenyl)-1-(2-methoxyphenyl)prop-2-en-1-one **4**

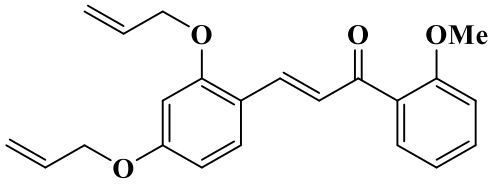

2,4-*Bis*(allyloxy)benzaldehyde (4.36 g, 20 mmol, M = 218.25 g/mol) and 2'-methoxyacetophenone (3.00 g, 20 mmol, M = 150.18 g/mol) were dissolved in ethanol (200 mL). The solution was cooled into ice and aq. KOH 40% (20 mL) was added. The solution was stirred at room temperature overnight. During the reaction, a precipitate formed. It was filtered off and washed with a minimum of ethanol. The solid was dissolved in DCM and the solution dried over magnesium sulfate. The solution was filtered on a plug of silicagel to remove the excess KOH and concentrated under reduced pressure. It was isolated as a light yellow solid (5.96 g, 85% yield). ^{1}H NMR ($CDCl_3$) δ : 3.86 (s,3H), 4.53-4.57 (m, 4H), 5.25-5.44 (m, 4H), 5.97-6.09 (m, 2H), 6.46 (d, 1H, J = 2.3 Hz), 6.52 (dd, 1H, J = 8.6 Hz, J = 2.3 Hz),6.96-7.04 (m, 2H), 7.31 (d, 1H, J = 16.0 Hz), 7.40-7.46 (m, 1H), 7.51 (d, 1H, J = 8.6 Hz), 7.56 (dd, 1H, J = 7.6 Hz, J = 1.7 Hz), 7.89 (d, 1H, J = 16.0 Hz); ^{13}C NMR ($CDCl_3$) δ : 55.7, 69.0, 69.1, 100.3, 106.5, 111.6, 117.5, 117.6, 118.1, 120.6, 125.5, 129.9, 130.1, 132.2? 132.7, 132.8, 139.4, 157.8, 159.0, 161.7, 193.9; HRMS (ESI MS) m/z: theor: 350.1518 found: 350.1515 ($M^{+\cdot}$ detected)

Synthesis of 3-(2,4-dibutoxyphenyl)-1-(2-methoxyphenyl)prop-2-en-1-one **5**

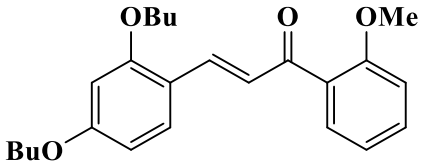

2,4-Dibutoxybenzaldehyde (5.00 g, 20 mmol, M = 250.34 g/mol) and 2'-methoxy-acetophenone (3.00 g, 20 mmol, M = 150.18 g/mol) were dissolved in ethanol (100 mL). Aq. KOH 40% (20 mL) was added and the solution was stirred at room temperature overnight. During the reaction, a precipitate formed. It was filtered off and washed with a minimum of ethanol. The solid was dissolved in DCM and the solution dried over magnesium sulfate. The solution was filtered on a plug of silicagel to remove the excess KOH and concentrated under reduced pressure. It was isolated as a light yellow solid (6.58 g, 86% yield). ^{1}H NMR ($CDCl_3$) δ : 0.91 (t, 3H, J = 7.4 Hz), 0.95 (t, 3H, J = 7.4 Hz), 1.39-1.50 (m, 4H), 1.70-1.79 (m, 4H), 3.85 (s, 3H), 3.95 (q, 2H, J = 6.3 Hz), 3.96 (q, 2H, J = 6.3 Hz), 6.39 (d, 1H, J = 2.3 Hz), 6.46 (dd, 1H, J = 8.6 Hz, J = 2.3 Hz), 6.93-7.01 (m, 2H), 7.24 (d, 1H, J = 16.1 Hz), 7.37-7.42 (m, 1H), 7.46-7.52 (m, 2H), 7.81 (d, 1H, J = 16.1 Hz); ^{13}C NMR ($CDCl_3$) δ : 13.8, 13.9, 19.2, 19.3, 31.2, 31.3, 55.7, 67.9, 68.1, 99.5, 105.9, 111.5, 117.0, 120.5, 125.1, 129.9, 130.1, 130.4, 131.9, 140.2, 157.7, 159.7, 162.5, 194.3; HRMS (ESI MS) m/z: theor: 382.2144 found: 382.2146 ($M^{+\cdot}$ detected)

Synthesis of 3-(4-(dodecyloxy)phenyl)-1-(3-methoxyphenyl)prop-2-en-1-one **6**

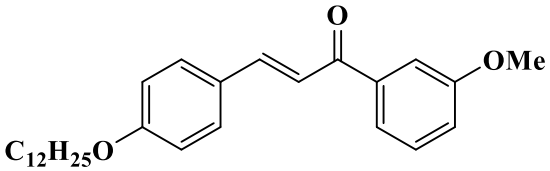

4-Dodecyloxybenzaldehyde (5.81 g, 20 mmol, M = 290.44 g/mol) and 3'-methoxyacetophenone (3.00 g, 20 mmol, M = 150.18 g/mol) were dissolved in ethanol (200 mL). The solution was cooled into ice and aq. KOH 40% (20 mL) was added. The solution was stirred at room temperature overnight. During the reaction, a precipitate formed. It was filtered off and washed with a minimum of ethanol. The solid was

dissolved in DCM and the solution dried over magnesium sulfate. The solution was filtered on a plug of silicagel to remove the excess KOH and concentrated under reduced pressure. It was isolated as a light yellow solid (6.17 g, 73% yield). ^{1}H NMR ($CDCl_3$) δ : 0.88 (t, 3H, J = 6.5 Hz), 1.22-1.48 (m, 18H), 1.79 (qt, 2H, J = 6.6 Hz), 3.88 (s, 3H), 3.99 (t, 2H, J = 6.7 Hz), 6.92 (d, 2H, J = 8.8 Hz), 7.09-7.13 (m, 1H), 7.35-7.42 (m, 2H), 7.53-7.54 (m, 1H), 7.57-7.60 (m, 3H), 7.78 (d, 1H, J = 15.6 Hz); ^{13}C NMR ($CDCl_3$) δ : 14.1, 22.7, 26.0, 29.2, 29.3, 29.4, 29.56, 29.59, 29.63, 29.66, 31.9, 55.5, 68.2, 112.9, 114.9, 119.0, 119.7, 120.9, 127.4, 129.5, 130.2, 140.0, 144.8, 159.9, 161.4, 190.3; HRMS (ESI MS) m/z: theor: 382.2144 found: 382.2142 ($M^{+\cdot}$ detected)

Synthesis of 3-(4-(dodecyloxy)phenyl)-1-(4-methoxyphenyl)prop-2-en-1-one **7**

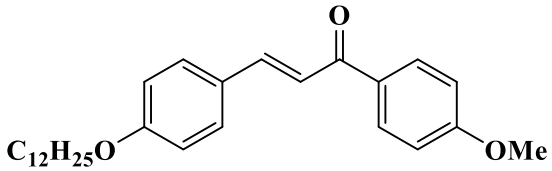

4-Dodecyloxybenzaldehyde (5.81 g, 20 mmol, M = 290.44 g/mol) and 4'-methoxy-acetophenone (3.00 g, 20 mmol, M = 150.18 g/mol) were dissolved in ethanol (200 mL). The solution was cooled into ice and aq. KOH 40% (20 mL) was added. The solution was stirred at room temperature overnight. During the reaction, a precipitate formed. It was filtered off and washed with a minimum of ethanol. The solid was dissolved in DCM and the solution dried over magnesium sulfate. The solution was filtered on a plug of silicagel to remove the excess KOH and concentrated under reduced pressure. It was isolated as a light yellow solid (7.44 g, 88% yield). ^{1}H NMR ($CDCl_3$) δ : 0.88 (t, 3H, J = 6.5 Hz), 1.22-1.48 (m, 18H), 1.82 (qt, 2H, J = 6.6 Hz), 3.89 (s, 3H), 4.00 (t, 2H, J = 6.7 Hz), 6.92 (d, 2H, J = 8.8 Hz), 6.98 (d, 2H, J = 8.9 Hz), 7.42 (d, 1H, J = 15.6 Hz), 7.58 (d, 2H, J = 8.8 Hz), 7.78 (d, 1H, J = 15.6 Hz), 8.03 (d, 2H, J = 8.9 Hz); ^{13}C NMR ($CDCl_3$) δ : 14.1, 22.7, 26.0, 29.2, 29.3, 29.4, 29.56, 29.58, 29.63, 29.65, 31.9, 55.5, 68.2, 113.8, 114.9, 119.5, 127.6, 130.1, 130.7, 143.9, 161.2, 163.3; HRMS (ESI MS) m/z: theor: 422.2821 found: 422.2824 ($M^{+\cdot}$ detected)

Synthesis of 3-(4-(diethylamino)-2-(dodecyloxy)phenyl)-1-(2-methoxyphenyl)prop-2-en-1-one **8**

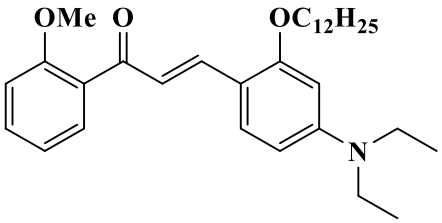

4-(Diethylamino)-2-(dodecyloxy)benzaldehyde (7.23 g, 20 mmol, M = 361.57 g/mol) and 2'-methoxy-acetophenone (3.00 g, 20 mmol, M = 150.18 g/mol) were dissolved in ethanol (100 mL). Aq. KOH 40% (20 mL) was added and the solution was stirred at room temperature overnight. During the reaction, a precipitate formed. It was filtered off and washed with a minimum of ethanol. The solid was dissolved in DCM and the solution dried over magnesium sulfate. The solution was filtered on a plug of silicagel to remove the excess KOH and concentrated under reduced pressure. It was isolated as a light orange solid (7.85 g, 79% yield). ^{1}H NMR ($CDCl_3$) δ : 7.83 (d, J = 15.9 Hz, 1H), 7.50 (dd, J = 7.5, 1.7 Hz, 1H), 7.43 (d, J = 8.8 Hz, 1H), 7.42 – 7.36 (m, 1H), 7.14 (d, J = 15.9 Hz, 1H), 7.02 – 6.94 (m, 2H), 6.27 (d, J = 8.8 Hz, 1H), 6.08 (d, J = 1.7 Hz, 1H), 3.96 (t, J = 6.4 Hz, 2H), 3.85 (s, 3H), 3.39 (q, J = 7.0 Hz, 4H), 1.81 – 1.73 (m, 2H), 1.45 – 1.36 (m, 2H), 1.29 (d, J = 15.9 Hz, 16H), 1.19 (t, J = 7.2 Hz, 6H), 0.89 (t, J = 6.8 Hz, 3H); ^{13}C NMR ($CDCl_3$) δ : 194.59, 160.44, 157.57, 151.15, 141.59, 131.41, 130.92, 130.80, 129.84, 122.18, 120.48, 111.92, 111.61, 104.56, 94.88, 68.28, 55.85, 44.71, 32.02, 29.79, 29.76, 29.75, 29.72, 29.67, 29.55, 29.46, 29.38, 26.25, 22.78, 14.20, 12.80, 12.71; HRMS (ESI MS) m/z: theor: 493.7320 found: 493.7318 ($M^{+\cdot}$ detected)

Synthesis of 3-(4-(dimethylamino)phenyl)-1-(2-methoxyphenyl)prop-2-en-1-one **9**

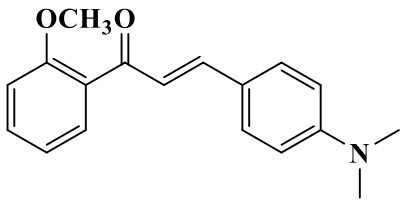

oui connu

4-(Dimethylamino)benzaldehyde (2.98 g, 20 mmol, M = 149.19 g/mol) and 2'-

methoxyacetophenone (3.00 g, 20 mmol, M = 150.18 g/mol) were dissolved in ethanol (100 mL). Aq. KOH 40% (20 mL) was added and the solution was stirred at room temperature overnight. During the reaction, a precipitate formed. It was filtered off and washed with a minimum of ethanol. The solid was dissolved in DCM and the solution dried over magnesium sulfate. The solution was filtered on a plug of silicagel to remove the excess KOH and the filtrate was concentrated under reduced pressure. It was isolated as a light orange solid (4.27 g, 76% yield). ^{1}H NMR ($CDCl_3$) δ : 7.57 – 7.51 (m, 2H), 7.47 (d, J = 8.9 Hz, 2H), 7.46 – 7.40 (m, 1H), 7.12 (d, J = 15.8 Hz, 1H), 7.02 (td, J = 7.5, 0.9 Hz, 1H), 6.98 (d, J = 8.4 Hz, 1H), 6.67 (d, J = 8.9 Hz, 2H), 3.88 (s, 3H), 3.02 (s, 6H); ^{13}C NMR ($CDCl_3$) δ : 193.64, 157.86, 152.05, 145.16, 132.08, 130.41, 130.40, 130.30, 130.11, 122.97, 122.56, 120.72, 112.00, 111.99, 111.76, 55.91, 40.26, 40.26; HRMS (ESI MS) m/z: theor: 281.1416 found: 281.1419 ($M^{+\cdot}$ detected)

Synthesis of 2,6-*bis*((*E*)-4-hydroxybenzylidene)cyclohexan-1-one **10**

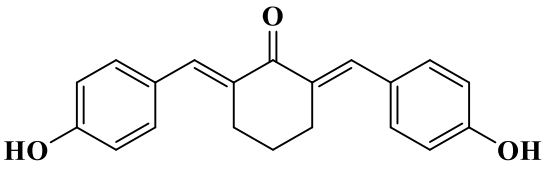

oui connu

4-Hydroxybenzaldehyde (2.44 g, 20 mmol, M = 122.12 g/mol) and cyclohexanone (0.98 g, 10 mmol, M = 98.15 g/mol) were dissolved in ethanol (100 mL). Aq. KOH 40% (20 mL) was added and the solution was stirred at room temperature overnight. During the reaction, a precipitate formed. It was filtered off and washed with a minimum of ethanol. The solid was dissolved in DCM and the solution dried over magnesium sulfate. The solution was filtered on a plug of silicagel to remove the excess KOH and the filtrate was concentrated under reduced pressure. It was isolated as a light orange solid (2.08 g, 68% yield). ^{1}H NMR (DMSO) δ: 9.71 (s, 2H), 7.54 (s, 2H), 7.40 (d, J = 8.6 Hz, 4H), 6.85 (d, J = 8.5 Hz, 4H), 2.85 (t, J = 5.3 Hz, 4H), 1.76 – 1.66 (m, 2H); ^{13}C NMR (DMSO) δ : 188.47, 158.55, 135.78, 133.19, 132.39, 126.27, 115.57, 27.94, 22.52; HRMS (ESI MS) m/z: theor: 728.4077 found: 728.4071 ($M^{+\cdot}$ detected).

Synthesis of 1-ferrocenyl-3-(2-thienyl)-2-propen-1-one **11**

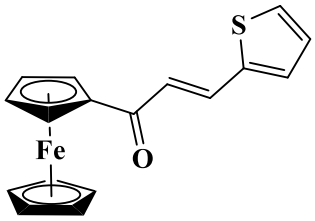

Acetylferrocene (3 g, 13.15 mmol, 1 equiv., M = 228.07 g/mol) and KOH (1 g, 13.15 mmol, 1 equiv., M= 56.11 g/mol) were dissolved in ethanol (20 mL) in a round bottomed flask. Thiophenecarboxaldehyde (2.40 g, 2 mL, 21.44 mmol, 1.5 equiv., M = 112.15 g/mol) in 10 mL EtOH was added dropwise and the mixture was stirred at room temperature for 24 h. The reaction was stopped by neutralizing the stirred solution with 2M HCl. A dark red precipitate after neutralization appeared, which was removed by filtration, washed with water and pentane. The solid was purified by column chromatography (SiO_2, Et_2O) giving the product (2.7 g, 60% yield) as red solid. Analytical data were consistent with those reported in the literature.[1] ^{1}H NMR ($CDCl_3$) δ : 7.90 (d, J = 15.4 Hz, 1H), 7.37 (d, J = 14.7 Hz, 2H), 7.09 (s, 1H), 6.92 (d, J = 15.3 Hz, 1H), 4.90 (s, 2H), 4.58 (s, 2H), 4.21 (s, 5H); ^{13}C NMR ($CDCl_3$) δ : 192.51, 140.67, 133.32, 131.39, 128.33, 127.89, 122.08, 80.62, 72.75, 70.13, 69.71; HRMS (ESI MS) m/z: theor: 322.0115 found: 322.0110 ($M^{+\cdot}$ detected)

Synthesis of 3-(furan-2-yl)-3-oxo-1-propen-1-yl]ferrocene **12**

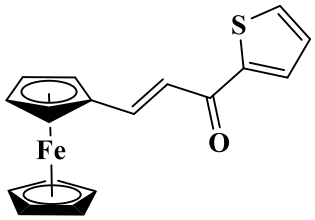

Acetylthiophene (1.18 g, 9.34 mmol, 1 equiv., M = 126.17 g/mol) and KOH (0.52 g, 9.34 mmol, 1 equiv., M = 56.11 g/mol) were dissolved in ethanol (20 mL) in a round bottomed flask. Ferrocenecarboxyaldehyde (2 g, 9.34 mmol, 1 equiv., M = 214.05 g/mol) was added and the mixture was stirred at room temperature for 24 h. The reaction was stopped by neutralizing the stirred solution with 2M HCl. A dark red precipitate

after neutralization appeared. It was then removed by filtration, washed with water, some cold ethanol, and pentane. The solid was purified by column chromatography (SiO2, Et2O) giving the product (2.36 g, 78% yield) as red solid. Analytical data were consistent with those reported in the literature.[2] ^{1}H NMR ($CDCl_3$) δ : 7.79 (d, J = 14.2 Hz, 2H), 7.65 (s, 1H), 7.16 (s, 1H), 7.03 (d, J = 15.1 Hz, 1H), 4.61 (s, 2H), 4.50 (s, 2H), 4.19 (s, 5H); ^{13}C NMR ($CDCl_3$) δ : 181.67, 146.10, 133.29, 131.26, 128.24, 118.86, 79.21, 71.61, 70.01, 69.21; HRMS (ESI MS) m/z: theor: 322.0115 found: 322.0111 ($M^{+\cdot}$ detected)

Synthesis of 1-ferrocenyl-3-(furan-2-yl)-2-propen-1-one **13**

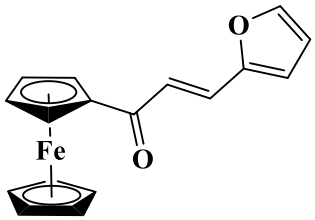

Acetylferrocene (3 g, 13.15 mmol, 1 equiv., M = 228.07 g/mol) and KOH (0.78 g, 14.02 mmol, 1.06 equiv., M = 56.11 g/mol) were dissolved in ethanol (20 mL) in a round bottomed flask. Furfural (1.35 g, 14.05 mmol, 1.07 equiv., M= 96.09 g/mol) was added dropwise and the mixture was stirred at room temperature for 24 h. The reaction was stopped by neutralizing the stirred solution with 2M HCl. a dark red precipitate appeared, which was removed by filtration, then washed with water and pentane. The solid was purified with column chromatography (SiO_2, Et_2O) giving the product (1.92 g, 45% yield) as a dark red powder. Analytical data were consistent with those reported in the literature.[4,1] ^{1}H NMR ($CDCl_3$) δ : 7.55 (d, J = 13.7 Hz, 2H), 7.04 (d, J = 14.9 Hz, 1H), 6.68 (s, 1H), 6.52 (s, 1H), 4.91 (s, 2H), 4.58 (s, 2H), 4.21 (s, 5H); ^{13}C NMR ($CDCl_3$) δ : 184.29, 152.45, 144.91, 127.63, 119.71, 115.93, 113.12, 82.58, 73.31, 70.67, 70.25; HRMS (ESI MS) m/z: theor: 306.0343 found: 306.0345 ($M^{+\cdot}$ detected)

Synthesis of 3-(furan-2-yl)-3-oxo-1-propen-1-yl]ferrocene **14**

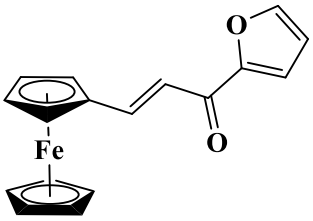

Acetylfurane (1.54 g, 14.02 mmol, 1 equiv., M = 214.05 g/mol) and KOH (0.78 g, 14.02 mmol, 1 equiv., M = 56.11 g/mol) were dissolved in ethanol (20 mL) in a round bottomed flask. Ferrocenecarboxyaldehyde (3 g, 14.02 mmol, 1 equiv., M = 214.05 g/mol) was added and the mixture was stirred at room temperature for 24 h. The reaction was stopped by neutralizing the stirred solution with 2 M HCl. a dark red precipitate after neutralization appeared which was removed by filtration and then washed with water, and pentane. The solid was purified by column chromatography (SiO_2, Et_2O) giving the product (2.62 g, 61% yield) as red powder. Analytical data were consistent with those reported in the literature.[2] ^{1}H NMR ($CDCl_3$) δ : 7.82 (d, J = 15.4 Hz, 1H), 7.63 (s, 1H), 7.27 (s, 1H), 7.04 (d, J = 15.5 Hz, 1H), 6.57 (s, 1H), 4.60 (s, 2H), 4.49 (s, 2H), 4.18 (s, 5H); ^{13}C NMR ($CDCl_3$) δ : 146.17, 118.47, 116.85, 112.52, 79.19, 71.59, 69.98, 69.24; HRMS (ESI MS) m/z: theor: 306.0343 found: 306.0348 ($M^{+\cdot}$ detected)

Synthesis of 3-(4-nitrophenyl)-3-oxo-1-propen-1-yl]ferrocene **15**

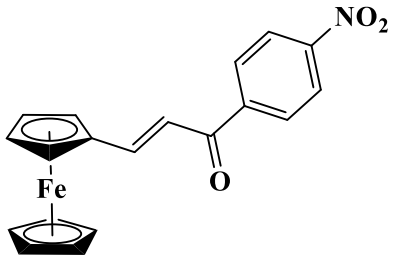

4-Nitroacetophenone (2.17 g, 13.15 mmol, M = 165.15 g/mol) and KOH (0.738 g, 13.15 mmol, M = 56.11 g/mol) were dissolved in ethanol (20 mL) in a round bottomed flask. Ferrocenecarboxyaldehyde (2.81 g, 13.15 mmol, M = 214.05 g/mol) was added and the mixture was stirred at room temperature for 24 h. The reaction was stopped by

neutralizing the stirred solution with 2M HCl. A violet precipitate after neutralization appeared. It was then removed by filtration, washed with water, some cold ethanol, and pentane. The obtained solid was chromatographied (SiO_2, Et_2O) giving the product (2.30 g, 45% yield) as a solid violet. Analytical data were consistent with those reported literature.[3] ^{1}H NMR ($CDCl_3$) δ : 8.33 (d, J = 5.2 Hz, 2H), 8.07 (d, J = 19.2 Hz, 2H), 7.81 (d, J = 14.8 Hz, 1H), 7.06 (d, J = 14.9 Hz, 1H), 4.64 (s, 2H), 4.57 (s, 2H), 4.22 (s, 5H); ^{13}C NMR ($CDCl_3$) δ 188.17, 149.56, 143.85, 129.37, 123.91, 118.37, 78.84, 72.34, 70.26, 69.60; HRMS (ESI MS) m/z: theor: 361.0401 found: 361.0406 ($M^{+\cdot}$ detected).

Synthesis of 1-ferrocenyl-3-(4-nitrophenyl)-2-propen-1-one **16**

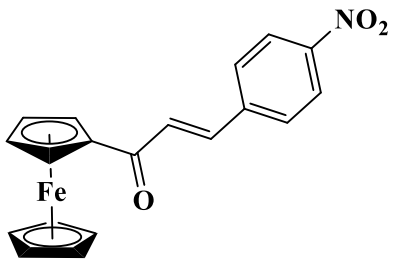

Acetylferrocene (2 g, 8.77 mmol, 1 equiv., M = 228.07 g/mol) and KOH (0.5 g, 8.91 mmol, 1.02 equiv., M = 56.11 g/mol) were dissolved in ethanol (20 mL) in a round bottomed flask. 4-nitrobenzaldehyde (1.33 g, 8.77 mmol, 1 equiv., M = 151.12 g/mol) was added and the mixture was stirred at room temperature for 24 h. The reaction was stopped by neutralizing the stirred solution with 2M HCl. A violet precipitate after neutralization appeared, which was separated by filtration, then washed with water, some cold ethanol, and pentane. The solid obtained was purified by column chromatography (SiO_2, Et_2O) giving the product (2.29 g, 72% yield) as violet powder. Analytical data were consistent with the literature.[4] ^{1}H NMR ($CDCl_3$) δ : 8.29 (d, J = 8.8 Hz, 2H), 7.79 (dd, J = 12.3, 5.6 Hz, 3H), 7.20 (d, J = 15.7 Hz, 2H), 4.99 – 4.88 (m, 2H), 4.72 – 4.62 (m, 2H), 4.24 (s, 5H); ^{13}C NMR ($CDCl_3$) δ : 192.28, 148.46, 141.67, 137.91, 128.89, 126.83, 124.37, 80.36, 73.47, 70.39, 69.99; HRMS (ESI MS) m/z: theor: 361.0401 found: 361.0402 ($M^{+\cdot}$ detected).

Synthesis of 3-(4-diphenylaminophenyl)-3-oxo-1-propen-1-yl]ferrocene **17**

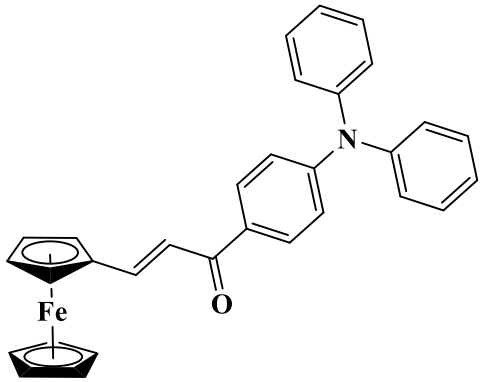

Ferrocenecarboxyaldehyde (0.92 g, 4.30 mmol, 1 equiv., M = 214.05 g/mol) and KOH (0.24 g, 4.30 mmol, 1 equiv., M = 56.11 g/mol) were dissolved in ethanol (20 mL) in a round bottomed. Then, 1-(4-Diphenylamino-phenyl)ethanone (1.24 g, 4.30 mmol, 1 equiv., M = 287.36 g/mol) was added dropwise and the mixture was stirred at room temperature for 24 h. The reaction was stopped by neutralizing the stirred solution with 2M HCl. a dark red precipitate after neutralization appeared. It was then removed by filtration, washed with water, and pentane. The crude solid was purified by column chromatography (SiO_2, Et_2O) giving the product (0.31 g, 15% yield) as a red solid. ^1H NMR ($CDCl_3$) δ : 7.89 – 7.85 (m, 2H), 7.81 – 7.69 (m, 2H), 7.33 – 7.29 (m, 6H), 7.18 – 7.11 (m, 4H), 7.08 – 6.95 (m, 2H), 4.59 (dd, J = 6.4, 4.6 Hz, 2H), 4.48 – 4.43 (m, 2H), 4.18 (d, J = 4.1 Hz, 5H); ^{13}C NMR ($CDCl_3$) δ : 187.43, 151.52, 146.34, 146.21, 145.04, 129.65, 129.29, 125.58, 124.22, 119.81, 79.28, 70.84, 69.46, 68.59; HRMS (ESI MS) m/z: theor: 484.1359 found: 484.1357 ($[M+H]^{+\cdot}$ detected)

Synthesis of 4-(*tert*-butyl)-2,6-*bis*(3-ferrocenylallylidene)cyclohexan-1-one **18**

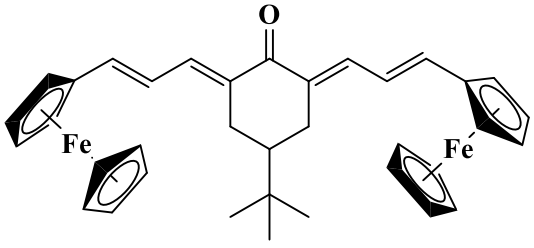

4-*tert*-Butylcyclohexanone (0.25 g, 1.62 mmol, 1 equiv., M = 154.25 g/mol) and KOH

(0.18 g, 3.24 mmol, 2 equiv., M= 56.11 g/mol) were dissolved in ethanol (15 mL) in a round bottomed flask. Ferroceneacrolein[5] (0.778 g, 3.24 mmol, 2 equiv., M = 240.08 g/mol) was added dropwise and the mixture was stirred at room temperature for 24 h. The reaction was stopped by neutralizing the stirred solution with 2M HCl. A dark red precipitate after neutralization appeared. It was then removed by filtration, washed with water and pentane. The solid obtained was purified by column chromatography (SiO_2, Et_2O) giving the product as red solid (0.2 g, 22% yield). ^{1}H NMR ($CDCl_3$) δ: 7.29 (dd, J = 11.6, 2.1 Hz, 2H), 6.75 (d, J = 15.0 Hz, 2H), 6.55 (dd, J = 15.1, 11.8 Hz, 2H), 4.42 (dd, J = 7.0, 1.5 Hz, 4H), 4.35 – 4.28 (m, 4H), 4.08 (s, 10H), 3.65 (dd, J = 13.9, 7.0 Hz, 1H), 2.86 (dd, J = 15.6, 3.1 Hz, 2H), 2.08 (t, J = 13.9 Hz, 2H), 0.98 (s, 9H); ^{13}C NMR ($CDCl_3$) δ : 189.58, 141.23, 136.82, 132.91, 121.49, 82.27, 70.34, 69.72, 68.01, 67.66, 43.52, 32.78, 27.94, 27.53; HRMS (ESI MS) m/z: theor: 598.1617 found: 598.1621 ($[M]^{+\cdot}$ detected)

---

[1] Villemin, D.; Martin, B.; Puciova, M.; Toma, S. Dry Synthesis under Microwave Irradiation: Synthesis of Ferrocenylenones. *Journal of Organometallic Chemistry* **1994**, *484* (1), 27–31. https://doi.org/10.1016/0022-328X(94)87181-7.

[2] Attar, S.; O'Brien, Z.; Alhaddad, H.; Golden, M. L.; Calderón-Urrea, A. Ferrocenyl Chalcones versus Organic Chalcones: A Comparative Study of Their Nematocidal Activity. *Bioorganic & Medicinal Chemistry* **2011**, *19* (6), 2055–2073. https://doi.org/10.1016/j.bmc.2011.01.048.

[3] Parveen, H.; Alatawi, R. A. S.; El Sayed, N. H.; Hasan, S.; Mukhtar, S.; Khan, A. U. Synthesis, Characterization and Biological Evaluation of Some Novel Nitrogen and Sulphur Containing Organometallic Heterocycles. *Arabian Journal of Chemistry* **2017**, *10* (8), 1098–1106. https://doi.org/10.1016/j.arabjc.2015.05.002.

[4] Liu, Y.-T.; Feng, L.; Yin, D.-W. The Catalysis, Synthesis and Characterization of Ferrocenylchalcone. *Research on Chemical Intermediates* **2013**, *39* (7), 2971–2977. https://doi.org/10.1007/s11164-012-0810-8.

[5] Plażuk, D.; Janowska, I.; Kłys, A.; Hameed, A.; Zakrzewski, J. A Convenient Synthesis of Conjugated ω-Arylpolyenals via Wittig Reaction with (1,3-Dioxan-2-Yl-Methyl)Triphenylphosphonium Bromide/Sodium Hydride. *Synthetic Communications* **2003**, *33* (3), 381–385. https://doi.org/10.1081/SCC-120015766.